

**CalciumSim: Simulator for calcium dynamics on neuron graphs  
using dimensionally reduced model**

---

A Thesis  
Submitted to  
the Temple University Graduate Board

---

in Partial Fulfillment  
of the Requirements for the Degree of  
MASTER OF SCIENCE

---

by  
Piyush Borole  
December, 2021

Examining Committee Members:

Gillian Queisser, Mathematics, Advisory Committee Chair  
Benjamin Seibold, Mathematics, Temple University  
Atilla Yilmaz, Mathematics, Temple University  
Joseph Picone, Engineering, Temple University

©

by

Piyush Borole

December, 2021

All Rights Reserved

**ABSTRACT**

CalciumSim: Simulator for calcium dynamics on neuron graphs using dimensionally reduced model

Piyush Borole

MASTER OF SCIENCE

Temple University, December, 2021

Gillian Queisser, Mathematics, Chair

Calcium signaling has been identified with triggering of gene transcriptions associated with learning and neuroprotection in neurons. Studies indicate that dysregulation of calcium signaling is correlated with severe Alzheimer Disease pathologies. A stable calcium wave or signal arising from triggers in dendritic synapses needs to reach soma with constant amplitude for proper functioning of neurons. In this study, we introduce “CalciumSim”, a calcium dynamics simulator which works on dimensionally reduced model. Numerical analysis is conducted to obtain the best configuration of neuron geometry to make the code efficient and fast. Alongside, biologically important insights are derived by modulating and changing parameters of the simulation. The ability of “CalciumSim” to work with real neuron geometries allows user to study calcium signalling in a realistic model.

## ACKNOWLEDGEMENTS

I begin thanking my advisor Dr Gillian Queisser, who has been a guide, mentor and support not only for my project but also through my entire masters program. I would like to thank James Rosado for his help in providing the neuron geometries and support in conceptualizing the implementation. Additionally his scripts for reading “.swc” file and making video has been extremely helpful for creating visualization. I would like to thank all my committee member for their time and suggestions. Finally, I want to thank my family and friends for their constant support through my MS journey.

To,

My Mom, Dad and sister, for being both, the warmth in  
my heart and light at the end of the tunnel.

# TABLE OF CONTENTS

<b>ABSTRACT</b>	<b>iv</b>
<b>ACKNOWLEDGEMENT</b>	<b>v</b>
<b>DEDICATION</b>	<b>vi</b>
<b>LIST OF FIGURES</b>	<b>ix</b>
<b>LIST OF TABLES</b>	<b>xi</b>
<b>1 Introduction</b>	<b>1</b>
1.1 Calcium Signalling . . . . .	1
1.2 Calcium dynamics . . . . .	2
1.2.1 Membrane transport mechanisms . . . . .	3
1.3 Dimensionality reduction . . . . .	8
1.4 Numerical Methods . . . . .	9
1.4.1 Forward Euler . . . . .	9
1.4.2 Backward Euler . . . . .	10
1.4.3 The Dormand-Prince pair method . . . . .	11
1.5 Method of Lines . . . . .	12
<b>2 Numerical Analysis</b>	<b>14</b>
2.1 Discretization . . . . .	14
2.1.1 Unbranched cable . . . . .	15
2.1.2 Branched cable . . . . .	16
2.1.3 End Points . . . . .	17
2.1.4 Implementation . . . . .	19
2.2 Choice of ODE solvers . . . . .	20
2.2.1 Diffusion PDE . . . . .	20
2.2.2 RyR channel ODE . . . . .	23

<b>3</b>	<b>Results</b>	<b>27</b>
3.1	Introduction . . . . .	27
3.2	Cytosolic $\text{Ca}^{2+}$ and CalB initial concentrations . . . . .	27
3.3	RyR Channels . . . . .	29
3.4	IP <sub>3</sub> R channels . . . . .	30
3.5	Concentration profiles . . . . .	33
3.6	Stable and abortive Calcium Wave . . . . .	34
3.7	Wave behaviour . . . . .	39
	3.7.1 Merging waves . . . . .	39
	3.7.2 Y-shaped neuron geometry . . . . .	40
3.8	Real neuron geometry . . . . .	45
<b>4</b>	<b>CalciumSim simulator</b>	<b>50</b>
4.1	Introduction . . . . .	50
4.2	“.swc” file . . . . .	52
4.3	$v_{l,e}$ , $v_{l,p}$ calculator . . . . .	53
4.4	time complexity . . . . .	55
<b>5</b>	<b>Conclusion</b>	<b>57</b>
	<b>REFERENCES</b>	<b>59</b>

# LIST OF FIGURES

1.1	Neuron Membrane Transport . . . . .	3
1.2	Method of Lines interpretation . . . . .	13
2.1	1D Unbranched cable . . . . .	15
2.2	1D Unbranched cable . . . . .	16
2.3	End point of cable, point $-1$ is a ghost point . . . . .	17
2.4	Branched cable Illustration . . . . .	19
2.5	Testing for spatial refinement needed for PDE discretization . . . . .	21
2.6	Testing for temporal refinement needed for Forward Euler . . . . .	23
2.7	Equilibrium probabilities of four state at varying Cytosolic $\text{Ca}^{2+}$ concentration . . . . .	24
2.8	Average step size needed for stability of ODE solver indicated that Implicit Backward Euler remains stable with larger step size for a range of cytosolic $\text{Ca}^{2+}$ concentration . . . . .	25
3.1	Open State Probability $p_R^o$ quickly approaches 1 as the cytosolic $\text{Ca}^{2+}$ concentration increases. . . . .	30
3.2	For most of the combinations of cytosolic $\text{Ca}^{2+}$ and $\text{IP}_3$ concentration, the $p_I^o$ is close to zero . . . . .	32
3.3	Variation in concentration profile behaviour with respect to increasing $k_p$ . . . . .	32
3.4	Concentration profiles with a stable wave progressing through the neuron . . . . .	34
3.5	Cable Neuron cytosolic $\text{Ca}^{2+}$ concentration profile at various time points indicating movement of $\text{Ca}^{2+}$ wave . . . . .	35
3.6	Effects of dendrite ( $R$ ) and ER ( $r$ ) on wave amplitude and velocity . . . . .	36
3.7	Effects of RyR density on amplitude and velocity . . . . .	38
3.8	Strong correlation between wave amplitude and velocity . . . . .	39

3.9	Calcium wave initiated on both end meeting at the center. <i>Left:</i> Cytosolic $\text{Ca}^{2+}$ concentration evolution over time in cable neuron. <i>Right:</i> ER $\text{Ca}^{2+}$ concentration evolution over time in cable neuron . . . . .	40
3.10	Wave progression in Y-shaped geometry when two end points are triggered . . . . .	42
3.11	Wave progression in Y-shaped geometry when one end point is triggered . . . . .	44
3.12	The cytosolic $\text{Ca}^{2+}$ concentration profiles at soma for 5 real neuron cell geometries. Each cell was triggered with randomly selected 10, 5 and 1 points . . . . .	47
3.13	Wave progression with 5 trigger points in Cell 1 . . . . .	48
3.14	Wave progression with 5 trigger points in Cell 2 . . . . .	48
3.15	Wave progression with 5 trigger points in Cell 3 . . . . .	48
3.16	Wave progression with 5 trigger points in Cell 4 . . . . .	49
3.17	Wave progression with 5 trigger points in Cell 5 . . . . .	49
4.1	Flowchart of CalciumSim: The red boxes indicates files from another author . . . . .	51
4.2	Constant ER $\text{Ca}^{2+}$ concentration at $250\mu\text{M}$ is seen when $v_{l,e,exact}$ is used. Using $v_{l,e,approx}$ leads to constant decrease in ER $\text{Ca}^{2+}$ concentration . . . . .	55
4.3	Time taken for one second of simulation on $1D$ neuron geometry made up of 2, 4, 8, 16, 32, 64, 128, 256, 512, 1024, 2048, 4096 points . . . . .	56

# LIST OF TABLES

1.1	Summary of mechanisms modelled in this study . . . . .	4
1.2	Parameters for simulation study . . . . .	7
3.1	Initial and Equilibrium Cytosolic $\text{Ca}^{2+}$ concentration . . . . .	29

# CHAPTER 1

## Introduction

### 1.1 Calcium Signalling

$\text{Ca}^{2+}$  signalling in neuron indicates biochemical response to a synaptic trigger. While the  $\text{Ca}^{2+}$  signalling occurs through the cytosol of neuron, in reality, the  $\text{Ca}^{2+}$  levels in cytosol at rest are very low. However, neurons employ plethora of mechanisms which modulates local  $\text{Ca}^{2+}$  concentration in cytosol leading to  $\text{Ca}^{2+}$  signalling toward soma. Reaching nucleus, this wave triggers gene transcriptions associated with learning and protecting neurons [22, 26, 28, 23, 17, 21, 31]. The study in [18] demonstrates pathway through which  $\text{Ca}^{2+}$  ions elicits response in nucleus.

The calcium transport mechanisms in neuron are enlisted in table 1.1 and illustrated in figure 1.1. Due to low  $\text{Ca}^{2+}$  concentrations in cytosol,  $\text{Ca}^{2+}$  stores in Endoplasmic Reticulum (ER) are utilized for creating stable  $\text{Ca}^{2+}$  signal [12, 2, 11, 27]. The ER is equipped with calcium exchange mechanisms such as ryanodine receptors channels (RyR), inositol 1, 4, 5-triphosphate ( $\text{IP}_3$ ) receptors and SERCA pumps for transporting  $\text{Ca}^{2+}$  ions across ER membrane. The RyR channels on the ER have a positive feedback property whereby the opening is facilitated by the presence of cytosolic calcium which triggers the release of even more calcium through surrounding channels. This is necessary as calcium signaling cannot be facilitate only by diffusion due to fast buffering

reaction [7]. Disruption in stable  $\text{Ca}^{2+}$  signalling is associated with neurodegeneration [4, 19, 14, 8]. Therefore learning how various parameters involved in calcium dynamics influences this signalling is vital to identify therapeutic targets. Previous studies study focused on simple neuron geometries involving cylindrical cable geometry [7, 6]. However, considering the complexity of neuron it is important to have a tool which implements calcium dynamics in real neuron geometry. In this study, we created a simulator ‘‘CalciumSim’’ in Matlab implementing diffusion and channel dynamics. It accepts any neuron geometry and reliably models calcium signalling for that neuron. Before testing on real geometry, it was tested on simple geometry involving long cable structure to ensure that results matches the previously done studies in [7].

## 1.2 Calcium dynamics

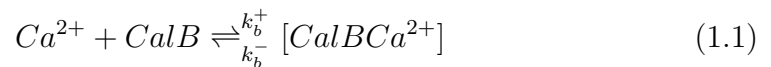
The calcium dynamics model studied here is obtained from [7, 6]. The primary spatio-temporal equations governing  $\text{Ca}^{2+}$  dynamics in neuron is by diffusion equation which are as follows:

$$\frac{\partial u}{\partial t} = \nabla \cdot (D \nabla u)$$

The one dimensional version of diffusion equation is

$$\frac{\partial u}{\partial t} = D \frac{\partial^2 u}{\partial x^2}$$

The four main chemical components involved in  $\text{Ca}^{2+}$  diffusion are cytosolic  $\text{Ca}^{2+}$ , Calbindin- $\text{D}_{28k}$  (CalB), Endoplasmic Reticulum (ER)  $\text{Ca}^{2+}$ , and Inositol 1,4,5- Triphosphate ( $\text{IP}_3$ ). The cytosolic  $\text{Ca}^{2+}$  and Calbindin- $\text{D}_{28k}$  (CalB) are present in cytosol and buffer each other. The ER  $\text{Ca}^{2+}$  present in ER do not interact chemically with any other species. Similarly,  $\text{IP}_3$  present in cytosol, does not chemically interact with either  $\text{Ca}^{2+}$  or CalB. The interaction between cytosolic  $\text{Ca}^{2+}$  and Calbindin- $\text{D}_{28k}$  (CalB) is given by:



Where  $k_b^+$  and  $k_b^-$  are association and disassociation constants. The values are mentioned in table 1.2 The diffusion equations for cytosolic calcium ( $c_c$ ), endoplasmic calcium ( $c_e$ ), Calbindin-D<sub>28k</sub> ( $b$ ) and IP<sub>3</sub> ( $p$ ):

$$\frac{\partial c_c}{\partial t} = D_c \Delta c_c + (k_b^- (b^{tot} - b) - k_b^+ b c_c) \quad (1.2)$$

$$\frac{\partial c_c}{\partial t} = D_c \frac{\partial^2 c_c}{\partial x^2} + (k_b^- (b^{tot} - b) - k_b^+ b c_c) \quad (1.3)$$

$$\frac{\partial b}{\partial t} = D_b \Delta b + (k_b^- (b^{tot} - b) - k_b^+ b c_c) \quad (1.4)$$

$$\frac{\partial c_e}{\partial t} = D_c \Delta c_e \quad (1.5)$$

$$\frac{\partial p}{\partial t} = D_p \Delta p - k_p (p - p^r) \quad (1.6)$$

The  $D_c$ ,  $D_b$  and  $D_p$  are diffusion constants for  $\text{Ca}^{2+}$ , CalB and IP<sub>3</sub> molecules. The  $p^r$  term is concentration of basal IP<sub>3</sub> in cytosolic space.  $k_p$  is the IP<sub>3</sub> molecule decay constant.  $b^{tot}$  is initial CalB concentration (remains constant throughout) and  $b^{tot} - b$  indicates CalB- $\text{Ca}^{2+}$  complex concentration. The initial and constant values are enlisted in table 1.2

### 1.2.1 Membrane transport mechanisms

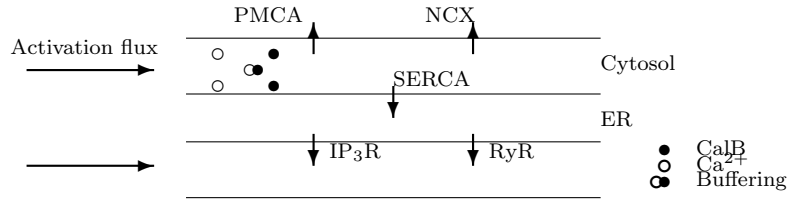


Figure 1.1: Neuron Membrane Transport

Regulation of  $\text{Ca}^{2+}$  ions in the cytosol of Neuron is regulated by various pumps and channels present over plasma membrane (PM) and endoplasmic reticulum membrane (ERM). The table 1.1 enlists pumps, channels and leakage terms modelled in this study. Figure 1.1 illustrates neurons along with its membrane transport mechanisms for  $\text{Ca}^{2+}$ .

Table 1.1: Summary of mechanisms modelled in this study

Name	Location	Flux Direction
IP <sub>3</sub> receptors (IP <sub>3</sub> R)	ERM	ER → Cytosol
Ryanodin receptors (RyR)	ERM	ER → Cytosol
Sarco/ER Ca <sup>2+</sup> -ATPase pumps (SERCA)	ERM	Cytosol → ER
Leakage	ERM	ER → Cytosol
plasma membrane Ca <sup>2+</sup> -ATPase pumps (PMCA)	PM	Cytosol → Extracellular space
Na <sup>+</sup> /Ca <sup>2+</sup> exchangers (NCX)	PM	ER Cytosol → Extracellular space
Leakage flux	PM	Extracellular space → Cytosol

The flux  $j_{ERM}$  forms flux over ER membrane constituting of  $j_I$ ,  $j_R$ ,  $j_S$  and  $j_{l,e}$  fluxes (from IP<sub>3</sub>R, RyR, SERCA and leakage flux respectively). Similarly, flux  $j_{PM}$  forms flux over PM constituting of  $j_P$ ,  $j_N$  and  $j_{l,p}$  (from PMCA, NCX and leakage flux).

$$j_{ERM} = j_I + j_R - j_S + j_{l,e} \quad (1.7)$$

$$j_{PM} = -j_P - j_N + j_{l,p} \quad (1.8)$$

Exchange mechanisms are assumed to be distributed uniformly for the simulation.

### IP<sub>3</sub>R channels

The Ca<sup>2+</sup> flux density generated by IP<sub>3</sub>R channels from ER to cytosol is calculated by

$$j_I = \rho_I \cdot p_I^o \cdot I_I \quad (1.9)$$

$$I_I = I_I^{ref} \frac{c_e - c_c}{c_e^{ref}} \quad (1.10)$$

$$p_I^o = \left( \frac{d_2 c_c p}{(c_c p + d_2 p + d_3 c_c + d_1 d_2)(c_c + d_5)} \right)^3 \quad (1.11)$$

where  $\rho_I$  is the IP<sub>3</sub>receptors density on the ER membrane,  $I_I$  is single channel Ca<sup>2+</sup>current and  $p_I^o$  is the probability that channel is in the open state. The model is obtained from [3] where  $I_I^{ref}$  is chosen to match ER Ca<sup>2+</sup>concentration at equilibrium (see table 1.2). Open state probability  $p_I^o$  is

calculated by equation 1.11 used from model stated in [9]. The parameters  $d_1$ ,  $d_2$ ,  $d_3$  and  $d_5$  given in table 1.2.

## RyR channels

The RyR channel flux density is calculated as follows:

$$j_R = \rho_R \cdot p_R^o \cdot I_R \quad (1.12)$$

$$I_R = I_R^{ref} \frac{c_e - c_c}{c_e^{ref}} \quad (1.13)$$

Where  $\rho_R$  is RyR channel density on ER membrane,  $I_R$  is single channel  $\text{Ca}^{2+}$  current and  $p_R^o$  is the probability that channel is in the open state. The model of open and closed state probability is governed by the following set ordinary differential equations obtained from [15]. This model proposes four state model with two open states  $o_1$  and  $o_2$  and two closed states  $c_1$  and  $c_2$  probabilities. The open state probability for channel is calculated as sum of the two open states  $o_1$  and  $o_2$ .

$$p_R^o = o_1 + o_2 \quad (1.14)$$

$$o_1 = 1 - o_2 - c_1 - c_2 \quad (1.15)$$

$$\frac{\partial c_1}{\partial t} = k_a^- o_1 - k_a^+ c_c^4 c_1 \quad (1.16)$$

$$\frac{\partial c_2}{\partial t} = k_c^+ o_1 - k_c^- c_2 \quad (1.17)$$

$$\frac{\partial o_2}{\partial t} = k_b^+ c_c^3 o_1 - k_b^- o_2 \quad (1.18)$$

$$\frac{\partial o_1}{\partial t} = -\frac{\partial o_2}{\partial t} - \frac{\partial c_1}{\partial t} - \frac{\partial c_2}{\partial t} \quad (1.19)$$

The values for  $k_a^\pm$ ,  $k_b^\pm$  and  $k_c^\pm$  are presented in table 1.2

## Pumps

### SERCA

The current from sarco/endoplasmic reticulum  $\text{Ca}^{2+}$ -ATPase or SERCA pumps

is described by following equation modelled after [24]. This was adapted for the one-dimensional case.

$$j_S = \rho_S \frac{I_S c_c}{(K_S + c_c) c_e} \quad (1.20)$$

The model is dependent on  $\text{Ca}^{2+}$  ion concentration in cytoplasm and endoplasmic reticulum. Parameters for the model is specified in table 1.2.

### PMCA

The plasma membrane  $\text{Ca}^{2+}$ -ATPase (PMCA) current is modelled as second-order Hill-equation adapted from [13]

$$j_P = \rho_P \frac{I_P c_c^2}{K_P^2 + c_c^2} \quad (1.21)$$

This model is dependent on cytosolic  $\text{Ca}^{2+}$  concentration. The values for the constants are presented in table 1.2

### NCX

The  $\text{Na}^+/\text{Ca}^{2+}$  exchanger current is modelled as first-order hill equation adapted from [13]. The  $\text{Na}^+$  concentration at the Plasma Membrane is assumed to be constant.

$$j_N = \rho_N \frac{I_N c_c}{K_N + c_c} \quad (1.22)$$

Similar to PMCA, NCX model is dependent only on cytosolic  $\text{Ca}^{2+}$  concentration. The values for the constants are presented in table 1.2

### Leakage

Endoplasmic reticulum membrane (ERM) and plasma membrane (PM) allows leakage of  $\text{Ca}^{2+}$  ions into cytosol. These leakage fluxes are modelled as  $j_{l,e}$  and  $j_{l,p}$  for Endoplasmic reticulum membrane and plasma membrane respectively.

$$j_{l,e} = v_{l,e} \cdot (c_e - c_c) \quad (1.23)$$

$$j_{l,p} = v_{l,p} \cdot (c_o - c_c) \quad (1.24)$$

Where  $c_e$  is ER  $\text{Ca}^{2+}$  concentration,  $c_c$  is cytosolic  $\text{Ca}^{2+}$  concentration and  $c_o$  is extracellular  $\text{Ca}^{2+}$  concentration (Constant value throughout, see table 1.2). The velocities  $v_{l,e}$  and  $v_{l,p}$  are calculated by setting net flux across ERM and PM zero at equilibrium. These values are presented in the table 1.2.

Table 1.2: Parameters for simulation study

Initial and Equilibrium values		SERCA pumps	
$c_c$	50 nM	$I_s$	$6.5 \times 10^{-21} \text{ mol } \mu\text{M}^{-1} \text{ s}^{-1}$
$c_e$	250 $\mu\text{M}$	$K_s$	180 nM
$c_o$	1 mM	$\rho_S$	$2390 \mu\text{m}^{-2}$
$b^{tot}$	40 $\mu\text{M}$	PMCA pump	
Diffusion/reaction		$I_P$	$1.7 \times 10^{-23} \text{ mol } \mu\text{M}^{-1} \text{ s}^{-1}$
$D_c$	$220 \mu\text{m}^2 \text{ s}^{-1}$	$K_P$	60 nM
$D_b$	$20 \mu\text{m}^2 \text{ s}^{-1}$	$\rho_P$	$500 \mu\text{m}^{-2}$
$D_p$	$280 \mu\text{m}^2 \text{ s}^{-1}$	NCX pumps	
$k_b^-$	$19 \text{ s}^{-1}$	$K_N$	1.8 $\mu\text{M}$
$k_b^+$	$27 \mu\text{M}^{-1} \text{ s}^{-1}$	$I_N$	$2.5 \times 10^{-21} \text{ mol } \text{ s}^{-1}$
$p$	40 nM	$\rho_N$	$15 \mu\text{m}^{-2}$
$k_p$	$10^3 \text{ s}^{-1}$	Leakage	
$p^r$	40 nM	$v_{l,e}$	$37.8 \text{ nm } \text{ s}^{-1}$
IP <sub>3</sub> R Channel		$v_{l,p}$	$4.49 \text{ nm } \text{ s}^{-1}$
$d_1$	0.13 $\mu\text{M}$	Ca <sup>2+</sup> /IP <sub>3</sub> release	
$d_2$	1.05 $\mu\text{M}$	$j_{SYNP}^c$	$2.5 \times 10^{-21} \text{ mol } \text{ s}^{-1} \mu\text{m}^{-2}$
$d_3$	0.94 $\mu\text{M}$	$\tau_c$	10 ms
$\rho_I$	$17.3 \mu\text{m}^{-2}$	$j_{SYNP}^p$	$5 \times 10^{-21} \text{ mol } \text{ s}^{-1} \mu\text{m}^{-2}$
$I_I^{ref}$	$1.1 \times 10^{-19} \text{ mol } \text{ s}^{-1}$	$\tau_p$	200 ms
$c_e^{ref}$	250 $\mu\text{M}$		
$d_5$	82.3 nM		
RyR Channels			
$k_a^-$	$28.8 \text{ s}^{-1}$		
$k_a^+$	$1500 \mu\text{M}^{-4} \text{ s}^{-1}$		
$k_b^-$	$385.9 \text{ s}^{-1}$		
$k_b^+$	$1500 \mu\text{M}^{-3} \text{ s}^{-1}$		
$k_c^-$	$0.1 \text{ s}^{-1}$		
$k_c^+$	$1.75 \text{ s}^{-1}$		
$\rho_R$	$3.0 \mu\text{m}^{-2}$		
$I_R^{ref}$	$3.5 \times 10^{-18} \text{ mol } \text{ s}^{-1}$		

## Calcium release and IP<sub>3</sub> production

Calcium activation is modelled as influx density entering the dendrite with value  $j_{SYNP} = 2.5 \times 10^{-18} \text{ mol } \mu\text{m}^{-2} \text{ s}^{-1}$  that linearly decreased to zero within 1 ms. IP<sub>3</sub> molecules are produced by calcium dependent AMPA receptor in the synapses [20]. The production of IP<sub>3</sub> molecules is also modelled as influx with initial strength  $5 \times 10^{-18} \text{ mol } \mu\text{m}^{-2} \text{ s}^{-1}$  linearly decreasing to zero over

200 ms as described in [6].

### 1.3 Dimensionality reduction

The diffusion problem associated with calcium dynamics is a three dimensional problem. However, we notice that the membrane mechanisms associated with calcium dynamics assumes that the channels and leakage occurs uniformly over the membrane. Essentially, the movement of fluxes through the membranes occurs uniformly over the ER and plasma membrane. Additionally, the  $\text{Ca}^{2+}$  released from ER diffuses almost instantaneously in the cross section of cytosol [7]. We make use of this rotational symmetry to reduce the three-dimensional problem to one-dimension along the axis of the neuron. To reduce the problem, we scale each term in diffusion equation with appropriate scaling factor. Let the dendrite radius be  $R$  and ER radius be  $r$ . The diffusion and reaction of cytosolic  $\text{Ca}^{2+}$ , CalB and  $\text{IP}_3$ , occurs in the cytosolic cross-section area at the point of interest. Therefore, they are scale by the factor equal to the cross-section area i.e.  $\pi(R^2 - r^2)$ . Since the ER  $\text{Ca}^{2+}$  diffusion term operates in ER only, they will be scaled with ER cross-sectional area i.e.  $\pi r^2$ . All the fluxes occurring over the plasma membrane and ER membrane are scaled by factor equal to circumference of dendrite i.e.  $2\pi R$  and ER i.e.  $2\pi r$  respectively. Effectively, we have following equations (Note, the direction along neuron axis is z-direction):

$$(R^2 - r^2) \frac{\partial c_c}{\partial t} = \frac{\partial}{\partial z} \left( (R^2 - r^2) D_c \frac{\partial c_c}{\partial z} \right) - (R^2 - r^2) (k_b^- (b^{tot} - b) - k_b^+ b c_c) + 2r j_{ERM} + 2R j_{PM} \quad (1.25)$$

$$r^2 \frac{\partial c_e}{\partial t} = \frac{\partial}{\partial z} \left( r^2 D_c \frac{\partial c_e}{\partial z} \right) - 2r j_{ERM} \quad (1.26)$$

$$(R^2 - r^2) \frac{\partial b}{\partial t} = \frac{\partial}{\partial z} \left( (R^2 - r^2) D_c \frac{\partial b}{\partial z} \right) - (R^2 - r^2) (k_b^- (b^{tot} - b) - k_b^+ b c_c) \quad (1.27)$$

$$(R^2 - r^2) \frac{\partial p}{\partial t} = \frac{\partial}{\partial z} \left( (R^2 - r^2) D_p \frac{\partial p}{\partial z} \right) \quad (1.28)$$

For the activation flux, as it enters in the cytosolic cross-section, it is also scaled with  $\pi(R^2 - r^2)$ .

## 1.4 Numerical Methods

Consider the following initial value problem between time span  $t_0$  to  $t_N$ :

$$Y'(t) = f(t, Y(t)) \dots (t_0 \leq t \leq t_N) \quad (1.29)$$

$$Y(t_0) = Y_0 \quad (1.30)$$

$$t_0 < t_1 < t_2 < \dots \leq t_N$$

$$t_n = t_0 + n\delta t \dots n = 0, 1, \dots, N$$

Now if this is a simple function, integration can yield a closed form solution. However, for complex problems such as the PDEs, ODE solvers are employed to integrate over time. In this section we consider three solvers - forward Euler, Backward Euler and Dormand-Prince Pair method.

### 1.4.1 Forward Euler

Forward Euler is an explicit method which calculates value at future time step using current time point. Consider the *forward difference approximation* for  $Y'$  as

$$Y'(t) \approx \frac{1}{\delta t} [Y(t + \delta t) - Y(t)] \quad (1.31)$$

$$Y(t + \delta t) = Y(t) + Y'(t)\delta t \quad (1.32)$$

$$(1.33)$$

The forward Euler being first order method has a local truncation error in the order of  $\mathcal{O}(h^2)$ . Furthermore, consider  $Y'(t) = \lambda Y(t)$ .

$$Y(t + \delta t) = Y(t) + Y'(t)\delta t \quad (1.34)$$

$$= Y(t) + Y(t)\delta t\lambda \quad (1.35)$$

$$= Y(t)(I + \lambda\delta t) \quad (1.36)$$

$$Y(t + 2\delta t) = Y(t)(I + \lambda\delta t)^2 \quad (1.37)$$

$$Y(t + n\delta t) = Y(t)(I + \lambda\delta t)^n \quad (1.38)$$

The forward Euler is stable only if  $|(I + \lambda\delta t)| < 1$  because anything  $\geq 1$  would lead the series to diverge. This means that forward Euler is only conditionally stable.

Due to such instability, often the choice of step size in forward Euler and other explicit methods are influenced by stability and not necessarily accuracy. When the explicit methods fails to work without taking extremely small steps, the problem is known as *stiff* problem [30, 25]. In such cases, as stability is the only issues, unconditionally stable implicit methods should be used instead.

### 1.4.2 Backward Euler

Backward Euler is an implicit method which calculates value at future time step using future time point itself.

$$Y(t + \delta t) = Y(t) + Y'(t + \delta t)\delta t \quad (1.39)$$

Consider  $Y'(t) = \lambda Y(t + \delta t)$ ,

$$Y(t + \delta t) = Y(t) + Y'(t + \delta t)\delta t \quad (1.40)$$

$$= Y(t) + Y(t + \delta t)\delta t\lambda \quad (1.41)$$

$$Y(t + \delta t)(I - \lambda\delta t) = Y(t) \quad (1.42)$$

$$Y(t + \delta t) = (I - \lambda\delta t)^{-1}Y(t) \quad (1.43)$$

$$Y(t + 2\delta t) = Y(t)(I - \lambda\delta t)^{-2} \quad (1.44)$$

$$Y(t + n\delta t) = Y(t)(I - \lambda\delta t)^{-n} \quad (1.45)$$

The Backward Euler is stable if  $|(I - \lambda\delta t)^{-1}| < 1$  or  $|(I - \lambda\delta t)| > 1$ . However,

$$|(I - \lambda\delta t)| > 1 \quad (1.46)$$

$$1 - \lambda\delta t > 1 \quad \text{or} \quad 1 - \lambda\delta t < -1 \quad (1.47)$$

$$\lambda\delta t < 0 \quad \text{or} \quad \lambda\delta t > 2 \quad (1.48)$$

$\delta t$  is always  $> 0$  and if we restrict  $\lambda < 1$  then  $\lambda\delta t < 0$  always. Therefore, backward Euler is unconditionally stable. The backward Euler being first order method has a local truncation error in the order of  $\mathcal{O}(h^2)$ .

### 1.4.3 The Dormand-Prince pair method

The Dormand-Prince pair method as described in [10] is a ODE solver of Runge-Kutta (RK) family. It forms a pair of explicit fourth-and fifth-order RK formula. The error between the fourth- and fifth order accurate solution are used for implementing an adaptive time-stepping scheme. One step of Dormand-Prince pair method consist of following steps [5, 16].

$$k_1 = hf(t_k, y_k) \quad (1.49)$$

$$k_2 = hf(t_k + \frac{1}{5}h, y_k + \frac{1}{5}k_1) \quad (1.50)$$

$$k_3 = hf(t_k + \frac{3}{10}h, y_k + \frac{3}{40}k_1 + \frac{9}{40}k_2) \quad (1.51)$$

$$k_4 = hf(t_k + \frac{4}{5}h, y_k + \frac{44}{45}k_1 - \frac{56}{15}k_2 + \frac{32}{9}k_3) \quad (1.52)$$

$$k_5 = hf(t_k + \frac{8}{9}h, y_k + \frac{19372}{6561}k_1 - \frac{25360}{2187}k_2 + \frac{64448}{6561}k_3 - \frac{212}{729}k_4) \quad (1.53)$$

$$k_6 = hf(t_k + h, y_k + \frac{9017}{3168}k_1 - \frac{355}{33}k_2 - \frac{46732}{5247}k_3 + \frac{49}{176}k_4 - \frac{5103}{18656}k_5) \quad (1.54)$$

$$k_7 = hf(t_k + h, y_k + \frac{35}{384}k_1 + \frac{500}{1113}k_3 + \frac{125}{192}k_4 - \frac{2187}{6784}k_5 + \frac{11}{84}k_6) \quad (1.55)$$

Next, we use these to calculate next step value of order 4 ( $y_{k+1,4}$ ) and order 5 ( $y_{k+1,5}$ ),

$$y_{k+1,4} = y_k + \frac{35}{382}k_1 + \frac{500}{1113}k_3 + \frac{125}{192}k_4 - \frac{2187}{6784}k_5 + \frac{11}{84}k_6 \quad (1.56)$$

$$y_{k+1,5} = y_k + \frac{5179}{57600}k_1 + \frac{7571}{16695}k_3 + \frac{393}{640}k_4 - \frac{92097}{339200}k_5 + \frac{187}{2100}k_6 + \frac{1}{40}k_7 \quad (1.57)$$

The difference between  $y_{k+1,5}$  and  $y_{k+1,4}$  gives us error estimate which can be used for calculating optimal step size ( $h_{opt}$ ).

$$|y_{k+1,5} - y_{k+1,4}| = \left| \frac{71}{57600}k_1 - \frac{71}{16695}k_3 + \frac{71}{1920}k_4 - \frac{17253}{339200}k_5 + \frac{22}{525}k_6 - \frac{1}{40}k_7 \right| \quad (1.58)$$

$$s = \left( \frac{\epsilon h_{old}}{2 \cdot |y_{k+1,5} - y_{k+1,4}|} \right)^{\frac{1}{5}} \quad (1.59)$$

$$h_{opt} = s h_{old} \quad (1.60)$$

Where  $h_{old}$  is the previous step size and  $\epsilon$  is user defined tolerance. It is provided as in-built function by Matlab known as ODE45. As an explicit method, it is accurate up to order four, but only on *nonstiff* problems. Dormand Prince pair method's local truncation error is  $\mathcal{O}(h^5)$ .

## 1.5 Method of Lines

Method of Lines is one of the techniques used for solving PDEs. In this technique, we discretize all the dimensions, except one, converting PDEs to ODE and then solving them using ODE solver. The figure 1.2 illustrates Method of Lines working. In our case, the diffusion PDEs have two dimensions, namely spatial and temporal. We discretized the spatial dimension such that left hand side of PDE can be calculated with known values. The progression in time is performed by some ODE solver such as Forward or Backward Euler.

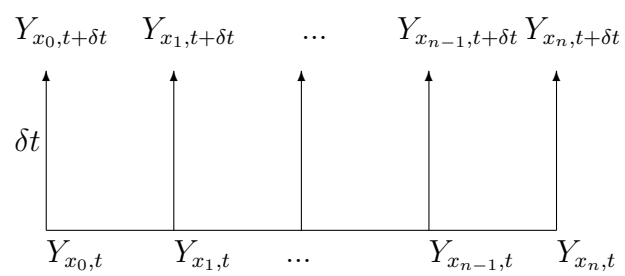


Figure 1.2: Method of Lines interpretation

# CHAPTER 2

## Numerical Analysis

### 2.1 Discretization

For diffusion PDEs, Method of Line described in section 1.5 is employed where left hand side derivatives are modelled as ODEs with right hand side discretized. Discretization of right hand side can be done by finite difference method. However, the neuron geometries we work with have unequal spacing between the points. Additionally, neurons geometries have branched structures. In order to solve our dimensionally reduced diffusion problem, we need to identify appropriate discretization scheme. First, discretization scheme for an unbranched cable geometry with unequally placed points is derived. Next, the discretization scheme is applied to branched cable. Lastly, discretization for end points is derived. Since the PDEs are diffusion equations, principle of mass conservation is applied for deriving appropriate discretization.

### 2.1.1 Unbranched cable

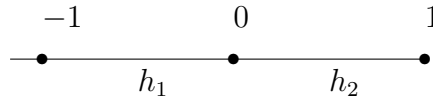


Figure 2.1: 1D Unbranched cable

For an 1D unbranched cable in fig. 2.1 We start with

$$accumulation = flux_{in} - flux_{out} \quad (2.1)$$

$$\frac{dM}{dt} = j_{-1 \rightarrow 0} - j_{0 \rightarrow 1} \quad (2.2)$$

Considering the 1D nature of the problem, here volume is length of neuron. In order to avoid double counting of  $h_1$  for  $C_0$  and  $C_{-1}$  calculations, we consider  $h_1/2$  as effective length on left of point 0. Similarly, we take  $h_2/2$  length on right side of point 0.

$$Mass = Concentration \times Length \quad (2.3)$$

$$M = C_0 \cdot \frac{h_1 + h_2}{2} \quad (2.4)$$

$$\frac{dM}{dt} = \frac{h_1 + h_2}{2} \cdot \frac{dC_0}{dt} \quad (2.5)$$

$$j_{-1 \rightarrow 0} = -D_c \frac{dC_{-1}}{dx} \dots \text{Fick's Law of diffusion} \quad (2.6)$$

$$j_{0 \rightarrow 1} = -D_c \frac{dC_1}{dx} \dots \text{Fick's Law of diffusion} \quad (2.7)$$

We substitute equations 2.5 – 2.7 in 2.2

$$\frac{h_1 + h_2}{2} \cdot \frac{dC_0}{dt} = D_c \cdot \left( \frac{dC_1}{dx} - \frac{dC_{-1}}{dx} \right) \quad (2.8)$$

$$\frac{h_1 + h_2}{2} \cdot \frac{dC_0}{dt} = D_c \cdot \left( \frac{C_1 - C_0}{h_2} - \frac{C_0 - C_{-1}}{h_1} \right) \quad (2.9)$$

$$\frac{h_1 + h_2}{2} \cdot \frac{dC_0}{dt} = D_c \cdot \left( \frac{C_{-1}}{h_1} - \left( \frac{1}{h_1} + \frac{1}{h_2} \right) \cdot C_0 + \frac{C_1}{h_2} \right) \quad (2.10)$$

$$\frac{dC_0}{dt} = \frac{2D_c}{h_1 + h_2} \cdot \left( \frac{C_{-1}}{h_1} - \left( \frac{1}{h_1} + \frac{1}{h_2} \right) \cdot C_0 + \frac{C_1}{h_2} \right) \quad (2.11)$$

This is for a general case where the spacing is uneven. If the spacing is even, we can set  $h_1 = h_2 = h$

$$\frac{dC_0}{dt} = \frac{D_c}{h^2} \cdot (C_{-1} - 2 \cdot C_0 + C_1) \quad (2.12)$$

This formula resembles second-order central difference formula with three-point stencil [1 2 1].

### 2.1.2 Branched cable

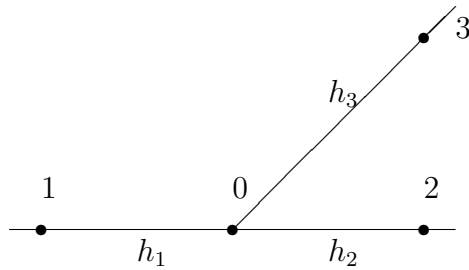


Figure 2.2: 1D Unbranched cable

Assuming influx from left and efflux from point 2 and 3, we employ similar approach for a branched cable by using mass conservation in fig. 2.2

$$\frac{dM}{dt} = j_{1 \rightarrow 0} - j_{0 \rightarrow 2} - j_{0 \rightarrow 3} \quad (2.13)$$

Here, since we have three neighbors adjoining 0, we take effective length as  $h_1/2 + h_2/2 + h_3/2$ .

$$M = C_0 \cdot \frac{h_1 + h_2 + h_3}{2} \quad (2.14)$$

$$\frac{dM}{dt} = \frac{h_1 + h_2 + h_3}{2} \cdot \frac{dC_0}{dt} \quad (2.15)$$

$$j_{1 \rightarrow 0} = -D_c \frac{dC_1}{dx} \dots \text{Fick's Law of diffusion} \quad (2.16)$$

$$j_{0 \rightarrow 2} = -D_c \frac{dC_2}{dx} \dots \text{Fick's Law of diffusion} \quad (2.17)$$

$$j_{0 \rightarrow 3} = -D_c \frac{dC_3}{dx} \dots \text{Fick's Law of diffusion} \quad (2.18)$$

We substitute 2.15 – 2.18 in 2.2,

$$\frac{h_1 + h_2 + h_3}{2} \cdot \frac{dC_0}{dt} = D_c \cdot \left( \frac{dC_2}{dx} + \frac{dC_3}{dx} - \frac{dC_1}{dx} \right) \quad (2.19)$$

$$\frac{h_1 + h_2 + h_3}{2} \cdot \frac{dC_0}{dt} = D_c \cdot \left( \frac{C_2 - C_0}{h_2} + \frac{C_3 - C_0}{h_3} - \frac{C_0 - C_1}{h_1} \right) \quad (2.20)$$

$$\frac{h_1 + h_2 + h_3}{2} \cdot \frac{dC_0}{dt} = D_c \cdot \left( \frac{C_1}{h_1} + \frac{C_2}{h_2} + \frac{C_3}{h_3} - \left( \frac{1}{h_1} + \frac{1}{h_2} + \frac{1}{h_3} \right) \cdot C_0 \right) \quad (2.21)$$

$$\frac{dC_0}{dt} = \frac{2D_c}{h_1 + h_2 + h_3} \cdot \left( \frac{C_1}{h_1} + \frac{C_2}{h_2} + \frac{C_3}{h_3} - \left( \frac{1}{h_1} + \frac{1}{h_2} + \frac{1}{h_3} \right) \cdot C_0 \right) \quad (2.22)$$

Thus, we obtain a general formula for calculating  $\frac{dC_i}{dt}$  for point  $i$ :

$$\frac{dC_i}{dt} = \frac{2D_c}{\sum_{j \in \mathcal{N}} h_j} \cdot \left( \sum_{j \in \mathcal{N}} \frac{C_j}{h_j} - \left( \sum_{j \in \mathcal{N}} \frac{1}{h_j} \right) \cdot C_i \right) \quad (2.23)$$

Where  $\mathcal{N}$  is set of neighboring points to  $i$ . This discretization scheme is used for Cytosolic Calcium, ER Calcium, CalB and IP<sub>3</sub> diffusion equations.

### 2.1.3 End Points

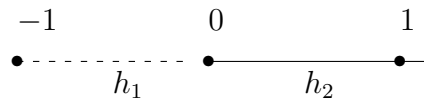


Figure 2.3: End point of cable, point  $-1$  is a ghost point

The end points are modelled with Neumann boundary condition. Consider the end point 0 and it's neighbor 1 at a distance  $h$ . In order to apply equation 2.12, we need to introduce a ghost point at  $-1$  from point 0 at a distance  $h$  such that distance between point  $-1$  and 1 is  $2h$  as in fig. 2.3

The Neumann Boundary condition is given as  $\frac{dC}{dx} = \alpha$ , where  $\alpha$  is some constant. From fick's first law of diffusion, we have,

$$j = -D \cdot \frac{dC}{dx} \quad (2.24)$$

$$\frac{dC}{dx} = -\frac{j}{D} \quad (2.25)$$

Where,  $j$  is an incoming or activation flux and  $D$  is diffusion coefficient. For our problem, we can use central difference for approximating  $\frac{dC_0}{dx}$  at point 0.

$$\frac{dC_0}{dx} = -\frac{j}{D} \quad (2.26)$$

$$\frac{C_1 - C_{-1}}{2h} = -j/D \quad (2.27)$$

$$C_{-1} = C_1 + 2h \cdot \frac{j}{D} \quad (2.28)$$

We will consider cytosolic  $\text{Ca}^{2+}$  diffusion equation here with diffusion constant  $D_c$ . Plugging this in 2.12,

$$\frac{dC_0}{dt} = \frac{D_c}{h^2} \cdot (C_{-1} - 2 \cdot C_0 + C_1) \quad (2.29)$$

$$\frac{dC_0}{dt} = \frac{D_c}{h^2} \cdot (C_1 + 2h \cdot \frac{j}{D_c} - 2 \cdot C_0 + C_1) \quad (2.30)$$

$$\frac{dC_0}{dt} = \frac{D_c}{h^2} \cdot (2 \cdot C_1 - 2 \cdot C_0) + 2 \cdot \frac{j}{h} \quad (2.31)$$

For neurons, the activation flux  $j$  is 0 when there is no trigger at that end point. The equation reduces to

$$\frac{dC_0}{dt} = \frac{D_c}{h^2} \cdot (2 \cdot C_1 - 2 \cdot C_0) \quad (2.32)$$

Or more generally,

$$\frac{dC_{endpt}}{dt} = \frac{D_c}{h^2} \cdot (2 \cdot C_{neighbor} - 2 \cdot C_{endpt}) \quad (2.33)$$

We use equation 2.31 with  $j = 0$  when end points are not triggered and  $j = \alpha$  when end point is triggered.

The same is true to ER  $Ca^{2+}$ , CalB and  $IP_3$  diffusion equation.

### 2.1.4 Implementation

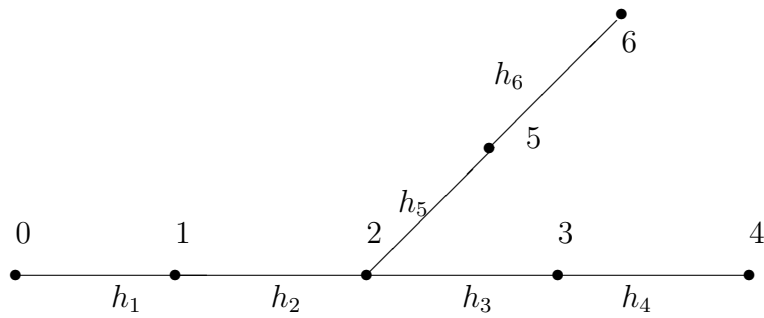


Figure 2.4: Branched cable Illustration

This type of discretization obtained in 2.23 and 2.33 allows us to vectorize the problem. For example, the branched cable in fig 2.4, the PDEs and be written as:

$$\begin{bmatrix} \frac{dC_0}{dt} \\ \frac{dC_1}{dt} \\ \frac{dC_2}{dt} \\ \frac{dC_3}{dt} \\ \frac{dC_4}{dt} \\ \frac{dC_5}{dt} \\ \frac{dC_6}{dt} \end{bmatrix} = \frac{2 \cdot D_c}{\sum_{i \in \mathcal{N}} h_i} *$$



tributing to accuracy.

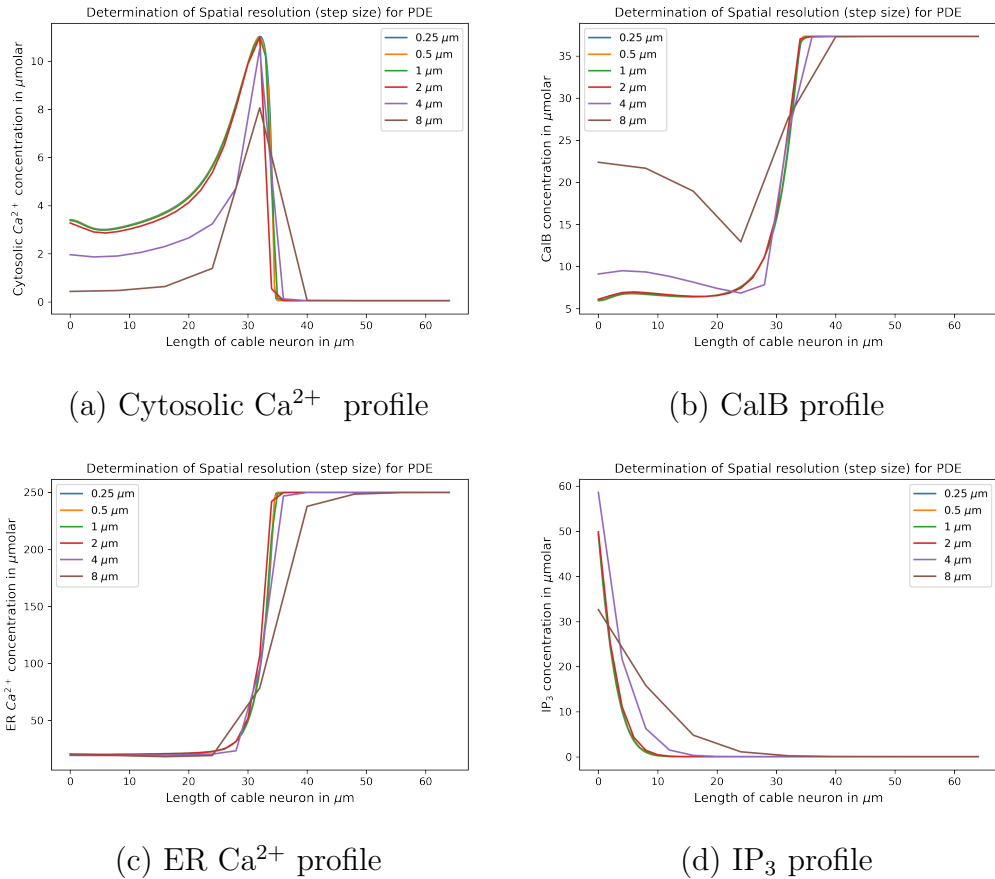


Figure 2.5: Testing for spatial refinement needed for PDE discretization

With this, the ODEs obtained from PDEs need to be integrated using an ODE solver. We explored explicit methods namely Forward Euler and Dormand-Prince pair method. With Forward Euler, temporal refinements were created with time steps  $25\mu\text{s}$ ,  $50\mu\text{s}$ ,  $100\mu\text{s}$ ,  $200\mu\text{s}$  and  $400\mu\text{s}$ . Same cable geometry was utilized and simulation was allowed to run for 500 milliseconds (Note: This is simulation time and not actual time taken for simulation). Concentration profile for first or left-most point over 500 milliseconds was plotted for cytoplasmic  $\text{Ca}^{2+}$ , CalB,  $\text{IP}_3$  and ER  $\text{Ca}^{2+}$  concentrations. As the refinement increases, concentration profiles converge to a

solution.  $100\mu s$  was identified to be the largest step size that can be chosen without compromising accuracy (See fig. 2.6). Note that for  $IP_3$  diffusion plot in fig. 2.6d, larger step sizes can also be selected without compromising accuracy. However, considering all four diffusion plots in fig. 2.6, step size of  $100\mu s$  was selected for Forward Euler method. Considering the high accuracy of Dormand-Prince pair method, the Matlab in-built function *ODE45* (Dormand-Prince implementation) was used for testing. There was no difference in solution between a forward Euler with step size  $100\mu s$  and *ODE45* with average step size  $1\mu s$  (but *ODE45* takes more iterations for integration). This is owing to the fact that *ODE45* as a default behavior will divide time steps into smaller fractions of  $1\mu s$  even when large deviations are not expected. Therefore, considering the fast yet accurate performance of forward Euler implementation, it was used as the ODE solver for discretized diffusion PDEs.

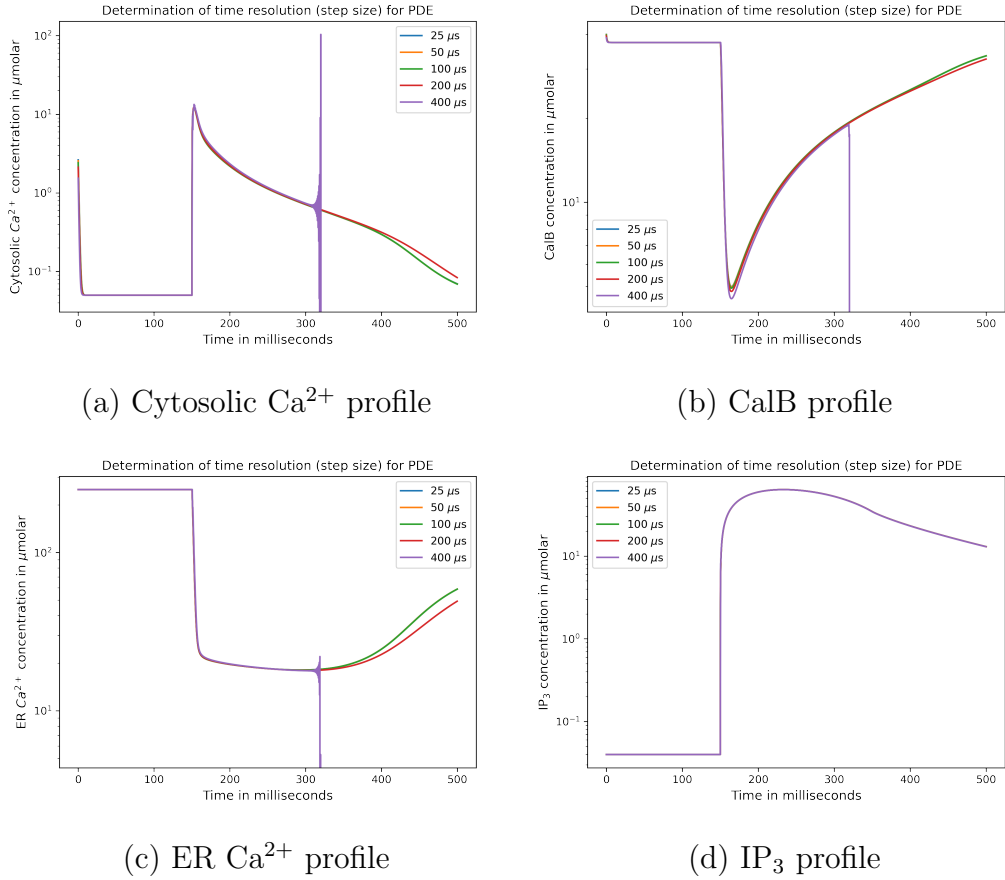


Figure 2.6: Testing for temporal refinement needed for Forward Euler

## 2.2.2 RyR channel ODE

For testing ODE solvers for RyR channel ODEs, we need equilibrium four-state probabilities as ground truth. At equilibrium, there is no change in probability states  $o_1$ ,  $o_2$ ,  $c_1$  and  $c_2$ . Consequently,

$$\frac{\partial c_1}{\partial t} = \frac{\partial c_2}{\partial t} = \frac{\partial o_1}{\partial t} = \frac{\partial o_2}{\partial t} = 0 \quad (2.35)$$

From equations 1.16 – 1.19, we also know that ODEs are dependent on cytosolic Ca<sup>2+</sup> concentration. Therefore, we can use equations 1.15 – 1.18 and 2.35 to create a system of linear equations to obtain equilibrium four-state probabilities at various concentrations of cytosolic Ca<sup>2+</sup>. The system of linear

equations is as follows:

$$\begin{bmatrix} 1 & 1 & 1 & 1 \\ k_a^- & 0 & -k_a^+ c_c^4 & 0 \\ k_b^+ c_c^3 & -k_b^- & 0 & 0 \\ k_c^+ & 0 & 0 & k_c^- \end{bmatrix} \begin{bmatrix} o_1 \\ o_2 \\ c_1 \\ c_2 \end{bmatrix} = \begin{bmatrix} 1 \\ 0 \\ 0 \\ 0 \end{bmatrix} \quad (2.36)$$

Fig. 2.7 demonstrates how the four states  $o_1$ ,  $o_2$ ,  $c_1$  and  $c_2$  of RyR channel varies with increasing concentration of cytosolic  $\text{Ca}^{2+}$ . As the concentration of cytosolic  $\text{Ca}^{2+}$  increases, the open state probability  $o_1$  approaches 1.

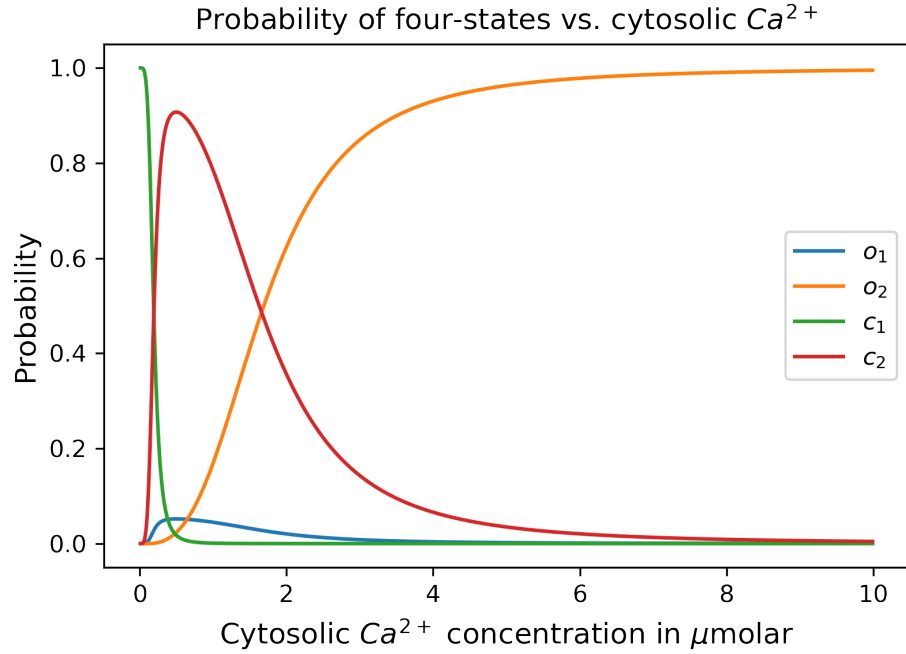


Figure 2.7: Equilibrium probabilities of four state at varying Cytosolic  $\text{Ca}^{2+}$  concentration

For the study, we considered Forward Euler, Dormand-Prince pair and Backward Euler described in 1.4.2 section. Of these, forward and backward Euler were implemented as described in sections 1.4.1 and 1.4.2 while for Dormand-Prince pair method, an in-built Matlab function ODE45 was utilized.

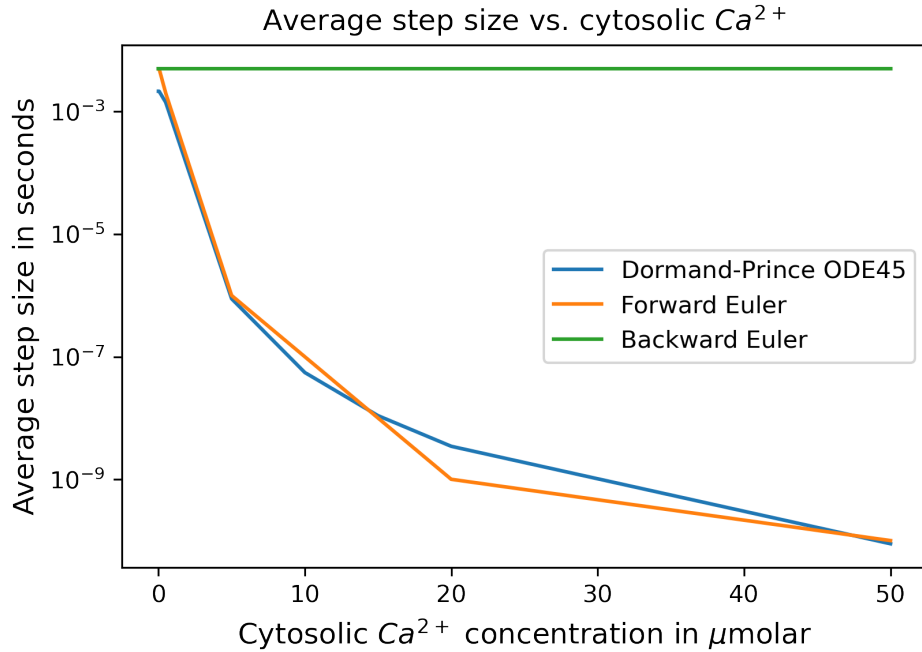


Figure 2.8: Average step size needed for stability of ODE solver indicated that Implicit Backward Euler remains stable with larger step size for a range of cytosolic  $Ca^{2+}$  concentration

Forward Euler method was employed for varying concentrations of cytosolic  $Ca^{2+}$ . However, it was noted that with an increase in cytosolic  $Ca^{2+}$  concentration, the step size needed for stability decreases. A similar trend was observed while using ODE45. While ODE45 utilizes adaptive stepping, the average step size calculated for a cytosolic  $Ca^{2+}$  concentration was in the range of Forward Euler step size. However, the step size required for stability in Backward Euler remained consistent over a range of cytosolic  $Ca^{2+}$  concentration (0.005 to 50  $\mu\text{M}$ ) as seen in fig. 2.8. The need to take smaller step sizes in explicit methods for stability indicates *stiffness* in ODEs. Therefore, Backward Euler which is stable and accurate over larger step sizes was chosen as ODE solver choice for RyR channel ODE. The step size needed in backward Euler for RyR channel ODE is well above  $100\mu\text{s}$  (See fig. 2.8, the step size needed for diffusion PDE.

This puts limits on the step size choice for RyR ODE. Therefore, in order to be consistent with PDE evolution, RyR channel ODE step size is also chosen to be  $100\mu s$ .

# CHAPTER 3

## Results

### 3.1 Introduction

Before running the simulator on real neuron geometries, the wave and system behaviour is studied on simple cable geometry. We consider a cable with  $L = 64\mu m$ , dendrite radius  $0.4\mu m$ , ER radius  $0.15\mu m$ , number of points 129 and distance between two adjacent points  $0.5\mu m$ . The initial and parameter values are taken from table 1.2. The activation flux is initiated after 150 ms of simulation time. The time between 0 – 150 ms is kept as buffer time for system to equilibrate.

### 3.2 Cytosolic $Ca^{2+}$ and CalB initial concentrations

The cytosolic  $Ca^{2+}$  and CalB diffusion equations (1.3 and 1.5 respectively) are couple together by a reaction term. As this reaction is a reversible reaction, the system reaches an equilibrium with equilibrium species concentrations different from initial values. However, the equilibrium concentrations are unique for each initial condition. From [7, 6], we want to maintain a equilibrium cytosolic  $Ca^{2+}$  concentration at  $c_c = 50$  nM. The initial cytosolic  $Ca^{2+}$  con-

centration is  $c_c^{init}$ , initial CalB concentration is  $b^{tot} = 40 \mu M$  and equilibrium CalB concentration is  $b$ . The concentration of CalB- $Ca^{2+}$  complex formed is  $c_c^{init} - c_c = b^{tot} - b$ . Considering these values, we can obtain initial cytosolic  $Ca^{2+}$  concentration. First we find an expression for equilibrium CalB concentration

$$\frac{\partial c_c}{\partial t} = D_c \frac{\partial^2 c_c}{\partial x^2} + (k_b^-(b^{tot} - b) - k_b^+ b c_c) \quad (3.1)$$

$$\frac{\partial c_c}{\partial t} = D_c \frac{\partial^2 c_c}{\partial x^2} = 0 \quad (3.2)$$

$$\dots \text{At equilibrium no change occurs} \quad (3.3)$$

$$k_b^-(b^{tot} - b) = k_b^+ b c_c \quad (3.4)$$

$$b = \frac{k_b^- b^{tot}}{k_b^- + k_b^+ c_c} \quad (3.5)$$

We can rewrite equation 3.4 as follows:

$$k_b^-(c_c^{init} - c_c) = k_b^+ b c_c \quad (3.6)$$

$$c_c^{init} = c_c + \frac{b^{tot} c_c k_b^+}{k_b^- + k_b^+ c_c} \quad (3.7)$$

$$\dots \text{substituting } b \text{ using eq. 3.5} \quad (3.8)$$

Substituting values from table 1.2 and  $c_c = 50 \text{ nM}$ , we find that the initial value is  $c_c^{init} = 2.703 \mu M$ . Simulations with a range of initial cytosolic  $Ca^{2+}$  values were performed for 0.1 second. The theoretical equilibrium values and simulation derived equilibrium values were obtained and compared in table 3.1. It was noted that the theoretical and simulation values were identical which demonstrates proper functioning of this couple system. Since the test was for the coupled cytosolic  $Ca^{2+}$  and CalB system, the pump mechanisms were turned off. As a sanity check of the implementation, for any simulation, the system was initialized with  $c_c^{init} = 2.703 \mu M$  initial value and allowed to equilibrate for 0.1 second before the pump mechanisms start to operate.

Table 3.1: Initial and Equilibrium Cytosolic  $\text{Ca}^{2+}$  concentration

Initial value	Theoretical equilibrium value	Simulation equilibrium value	Error
5 $\mu\text{M}$	0.0982	0.0982	$2.02E - 07$
4 $\mu\text{M}$	0.0765	0.0765	$3.62E - 07$
3 $\mu\text{M}$	0.0559	0.0559	$2.36E - 07$
2.703 $\mu\text{M}$	0.05	0.05	$1.67E - 16$
2 $\mu\text{M}$	0.0363	0.0363	$4.65E - 07$
1 $\mu\text{M}$	0.0177	0.0177	$3.53E - 10$
0.5 $\mu\text{M}$	0.0087	0.0087	$2.30E - 08$

### 3.3 RyR Channels

The RyR channels open state probability is governed by set of ODEs (Eq. 1.16 – 1.19) which are cytosolic  $\text{Ca}^{2+}$  dependent. Plot in figure 3.1 demonstrates the switch like nature of RyR channels open probability ( $p_R^o$ ). Once the cytosolic  $\text{Ca}^{2+}$  concentration reaches a certain threshold (approximately 4  $\mu\text{M}$ ), the open state probability shoots to 1. This is vital for calcium wave. The RyR channels dynamics takes places at much smaller time scale compared to diffusion and  $\text{IP}_3\text{R}$  mechanism. Therefore, for the progression and sustenance of stable wave, immediate release of  $\text{Ca}^{2+}$  ions into cytosol is needed. This process is mediated by RyR channels which allow massive bursts of  $\text{Ca}^{2+}$  ions flux from ER  $\text{Ca}^{2+}$  stores after sensing increase in cytosolic  $\text{Ca}^{2+}$  concentration.

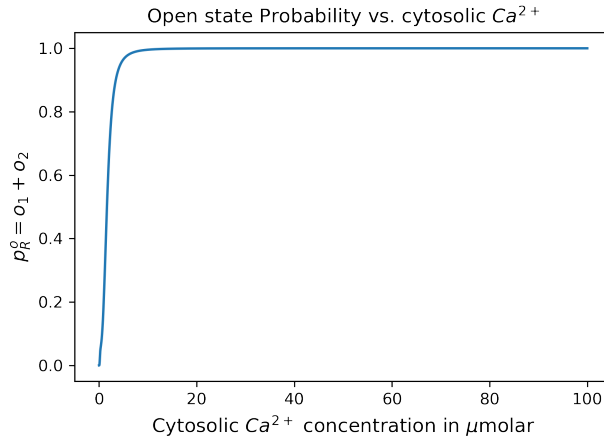


Figure 3.1: Open State Probability  $p_R^o$  quickly approaches 1 as the cytosolic  $\text{Ca}^{2+}$  concentration increases.

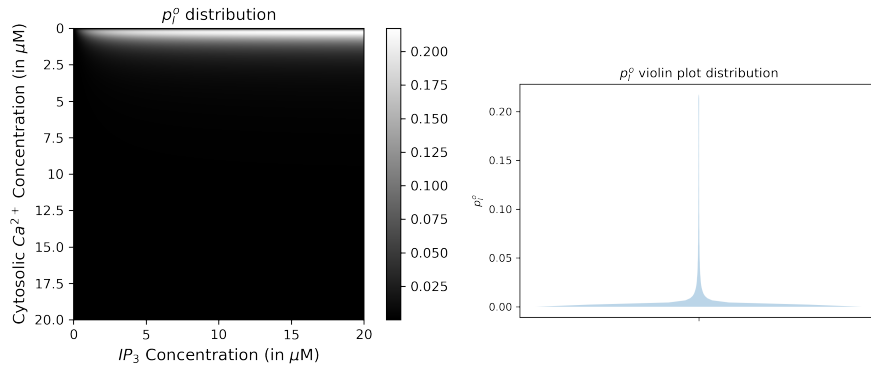
### 3.4 IP<sub>3</sub>R channels

Along with RyR channels, IP<sub>3</sub>R channel modulates the dynamics to ensure progression of stable  $\text{Ca}^{2+}$  wave. From equation 1.11 it can be seen that the open state probability of IP<sub>3</sub>R channels are dependent on the cytosolic  $\text{Ca}^{2+}$  and IP<sub>3</sub> concentrations.

Open state probability  $p_I^o$  for various combinations of cytosolic  $\text{Ca}^{2+}$  and IP<sub>3</sub> was calculated. Concentration ranging from 0 to 20  $\mu\text{M}$  with the step size of 0.01  $\mu\text{M}$  for each were used to calculate  $p_I^o$ . In total, four million combinations or probabilities were calculated and plotted in subfigure 3.2a. As seen in the violin plot figure 3.2b, most of the concentration values are close to zero (In the range of  $10^{-4}$ ). Very few combinations raises  $p_I^o$  to the range of 0.1 – 0.2. This is also seen in figure 3.2a where a thin light band of high probability area is seen surrounded by very low probability area plot. This means that the IP<sub>3</sub>R channels, similar to RyR channels, demonstrates “on-off” states with a very narrow range for “on” state. The concentration range for cytosolic  $\text{Ca}^{2+}$  and IP<sub>3</sub> for “on” probability is 0.1 – 2  $\mu\text{M}$  and 0.1 – 20

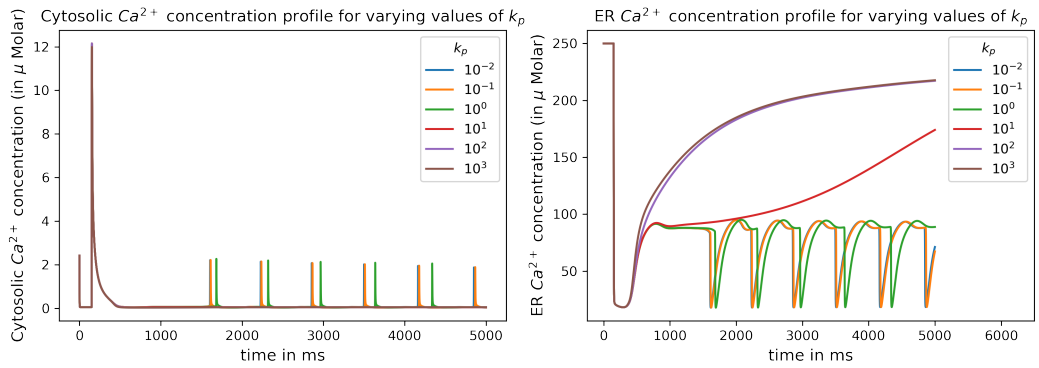
$\mu M$ .

Noticing the top most part of subfigure 3.2a, we note that before the light region begins, there is a very thin region of low probability (almost zero). This leads to an interesting phenomenon when the  $IP_3$  molecule decays slowly. The decay of  $IP_3$  molecule is influenced by  $k_p$ , where low value allows sustained higher concentration of  $IP_3$ . Consider a situation where the concentration of  $IP_3$  molecule is around  $5\mu M$  and is sustained for a long time due to smaller value of  $k_p$ . With equilibrium  $Ca^{2+}$  concentration of  $0.05\mu M$ , the  $p_I^o$  is close to zero. However, as a calcium wave passes, the cytosolic  $Ca^{2+}$  concentration shoots up to  $11\mu M$  while passing through high probability zone. But, once the wave passes and the cytosolic  $Ca^{2+}$  concentration starts decreasing, it again enters the zone of higher probability which leads to massive  $IP_3R$  flux. This again causes cytosolic  $Ca^{2+}$  concentration to increase and the cycle continues until the  $IP_3$  molecule decays entirely. This can be seen in subfigure 3.3a where after a massive jump in cytosolic  $Ca^{2+}$  concentration (caused by wave) there are periodic but shorter increases in cytosolic  $Ca^{2+}$  concentration when  $k_p$  is low. This is also seen in ER  $Ca^{2+}$  concentration in subfigure 3.3b where after a massive dip (caused by wave) there is periodic dip in concentration as soon as ER  $Ca^{2+}$  concentration starts increasing. However, we note that as the  $k_p$  increases, the  $IP_3$  molecule decays sooner allowing cytosolic  $Ca^{2+}$  concentration to decline without passing through high  $p_I^o$  zone. It is also seen that the ER is able to replenish its  $Ca^{2+}$  stores without losing them to  $IP_3R$  channels. However, beyond  $k_p = 10^3 s^{-1}$ , the rate at which replenishment of ER  $Ca^{2+}$  does not increase. For our simulations, we set the  $k_p$  value to  $10^3 s^{-1}$ .



(a)  $p_I^o$  distribution as function of cytosolic  $\text{Ca}^{2+}$  and  $\text{IP}_3$  concentration (b) Violin plot distribution of  $p_I^o$

Figure 3.2: For most of the combinations of cytosolic  $\text{Ca}^{2+}$  and  $\text{IP}_3$  concentration, the  $p_I^o$  is close to zero

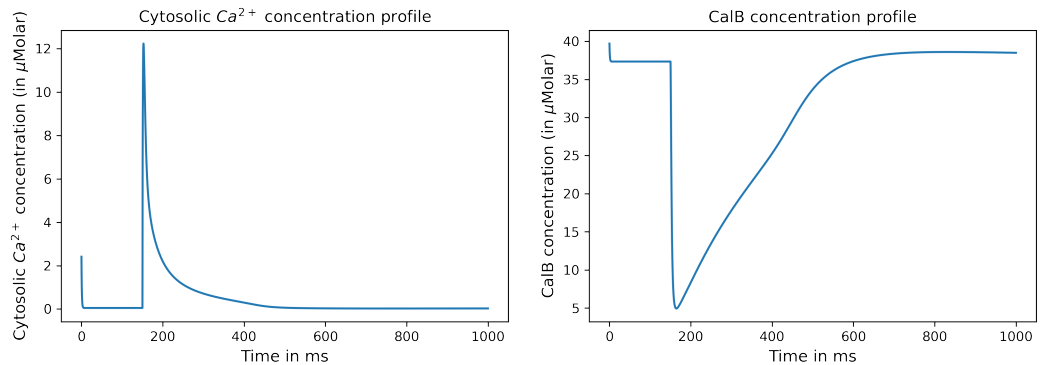


(a) Cytosolic  $\text{Ca}^{2+}$  concentration profile over time (b) ER  $\text{Ca}^{2+}$  concentration profile over time

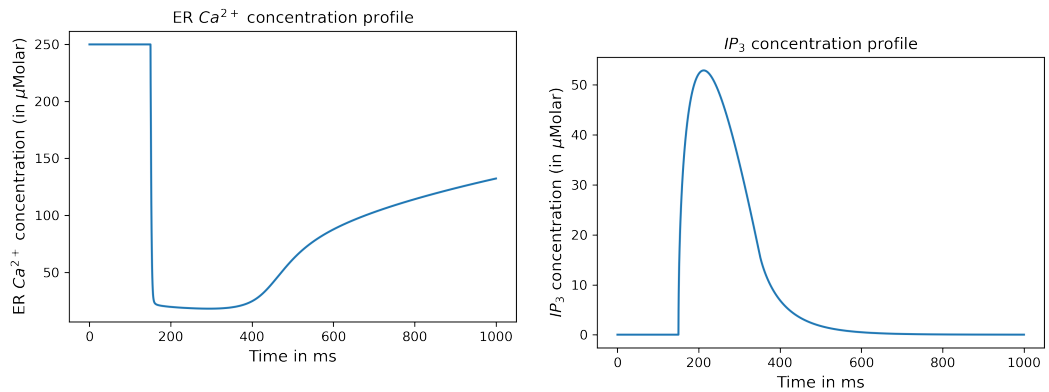
Figure 3.3: Variation in concentration profile behaviour with respect to increasing  $k_p$

### 3.5 Concentration profiles

In order to understand wave mechanics, it is important to understand how the wave affects concentration profile for cytosolic  $\text{Ca}^{2+}$ , CalB, ER  $\text{Ca}^{2+}$  and  $\text{IP}_3$  for the point where the wave passes through. The concentration profiles are plotted for the midpoint in the cable geometry. The simulation time is 1000 ms. The first subfigure 3.4a shows that when the wave reaches the point, there is a sharp increase in cytosolic  $\text{Ca}^{2+}$  concentration followed by exponential decrease over time. This sharp increase creates an imbalance in the CalB- $\text{Ca}^{2+}$  reaction equilibrium pushing forward reaction. This is associated with sharp decline in CalB concentration (see subfigure 3.4b) followed by steady increase as pump mechanisms start removing extra  $\text{Ca}^{2+}$  ions from cytosol. The increase in cytosolic  $\text{Ca}^{2+}$  concentration is mediated by RyR and  $\text{IP}_3\text{R}$  channels which immediately transports  $\text{Ca}^{2+}$  from ER to cytosol leading to exhaustion of ER  $\text{Ca}^{2+}$  (see subfigure 3.4c). However, the replenishment of ER  $\text{Ca}^{2+}$  mediated by SERCA pumps is a slow process and the concentration does not rise to equilibrium value for a very long time. This creates  $\text{Ca}^{2+}$  deficiency in ER for a long time. We also see that  $\text{IP}_3$  concentration rising as a result of diffusion but decays to equilibrium values. This decay is rapid as a result of  $k_p = 10^3 \text{s}^{-1}$ .



(a) Cytosolic  $\text{Ca}^{2+}$  concentration profile over time (b) CalB  $\text{Ca}^{2+}$  concentration profile over time



(c) ER  $\text{Ca}^{2+}$  concentration profile over time (d)  $\text{IP}_3$  concentration profile over time

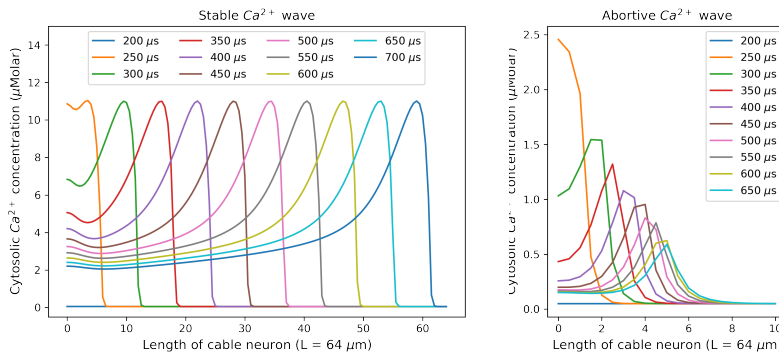
Figure 3.4: Concentration profiles with a stable wave progressing through the neuron

### 3.6 Stable and abortive Calcium Wave

The conditions needed for stable calcium wave moving from one end of cable neuron to other is described in [7]. This study does an exhaustive search to identify suitable conditions needed for sustaining a stable wave. However, this study focuses only on a cable geometry with equally spaced points. In

order to ensure that our simulator (CalciumSim) works as expected, we use a cable neuron geometry with  $L = 64\mu M$  and compared the plots generated with the plots in [7]. To match the [7] study, radius of dendrite and ER is kept constant for the entire neuron. It was noted that due to few differences in the model we implement versus the study (For instance, [7] does not implement IP<sub>3</sub>R channels but we do), the exact values may not match but the trend and behaviour of components is consistent.

The first plot we look at is an example of stable calcium wave and abortive wave. Figure 3.5a demonstrates an example of stable  $Ca^{2+}$  wave moving through the neuron. When a wave is stable, amplitude of the wave remains constant throughout. Whereas in abortive waves, the amplitude rapidly decreases well below the RyR channel triggering levels which stalls the wave.



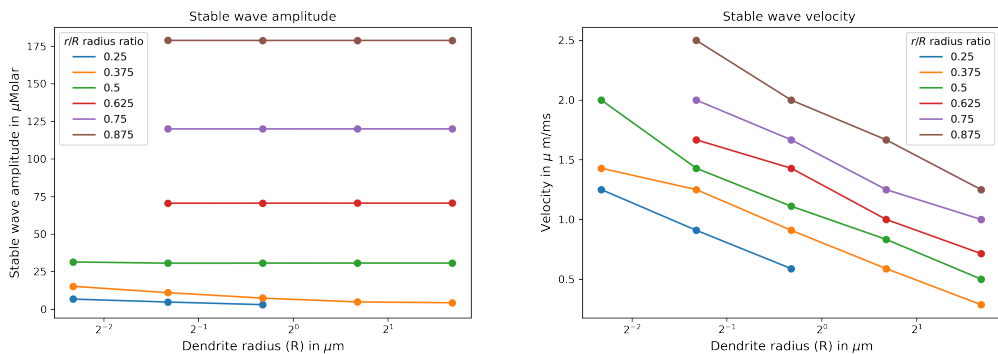
(a) Example of a stable wave

(b) Example of an abortive wave

Figure 3.5: Cable Neuron cytosolic  $Ca^{2+}$  concentration profile at various time points indicating movement of  $Ca^{2+}$  wave

Next, we were interested in studying the effects of changing dendrite and ER radius on the wave behaviour, specifically on amplitude and velocity. We want to work with real neuron geometries which has uneven dendrite radius. Therefore, it is important to study the behaviour on simpler geometry to predict its effects in real geometry. For this purpose, we utilized the same cable

geometry but with dendrite radius values 0.2, 0.4, 0.8, 1.6 and 3.2  $\mu\text{m}$ . Since actual value of ER radius did not inform a lot about wave behaviour, we considered looking at the ER radius to dendrite radius ratio ( $r$  and  $R$  respectively). We noticed that as the ER/dendrite radius ( $r/R$ ) ratio increases, the amplitude and velocity of the stable wave increases (see figure 3.6). From subfigure 3.6a, we see that while higher radius ratio leads to faster wave progression, overall, increase in dendrite radius leads to decreasing of wave velocity. With respect to amplitude, the value remains relatively constant for a particular radius ratio.

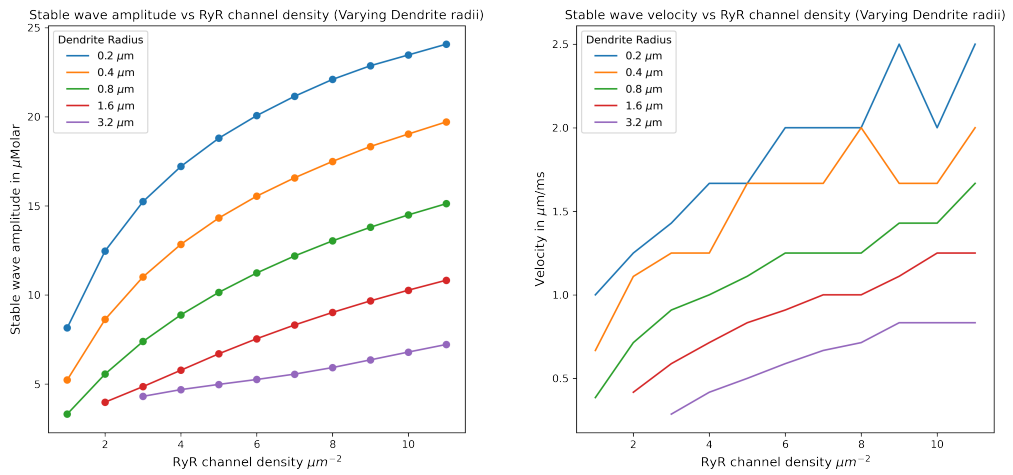


(a) Amplitude change with respect to  $r$  and  $R$  (b) Velocity change with respect to  $r$  and  $R$

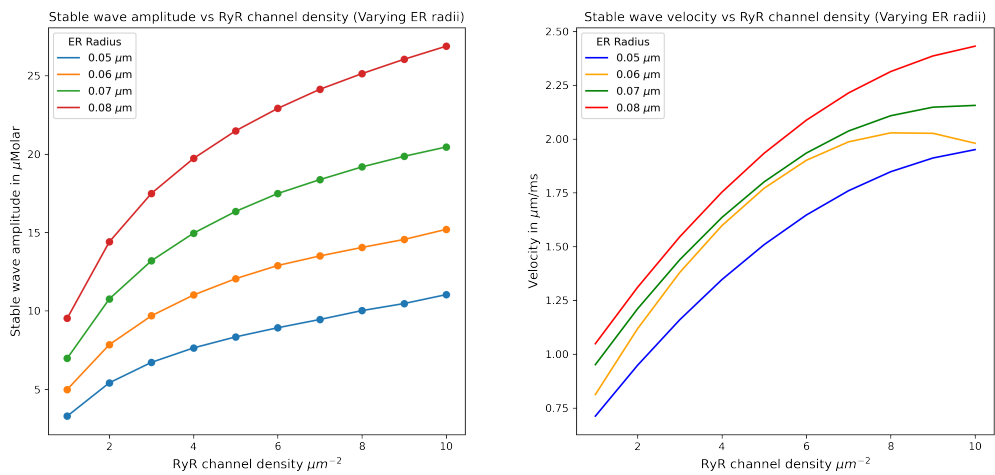
Figure 3.6: Effects of dendrite ( $R$ ) and ER ( $r$ ) on wave amplitude and velocity

Further, as the RyR channels plays an important part in stable wave, [7] indicates that RyR density plays an important part in amplitude and velocity of the wave. We conducted a series of experiments with changing RyR channel density along with changing dendrite radius and ER radius (see figure 3.7). When experimenting with changing dendrite radius, ER radius is selected by multiplying dendrite radius with a specific ratio ( $r/R = 0.375$ ). This ratio was selected considering the ability to produce stable wave over wide range of dendrite radius. Whereas, while experimenting with changing ER radius, a constant dendrite radius of  $0.2\mu\text{m}$  was selected to match [7] study.

Overall, as the RyR density increases, the wave amplitude and velocity increases (See figure 3.7). The two amplitude plots (subfigures 3.7a, 3.7c) shows quasi-linear increase with respect to RyR density. However, the wave amplitude decreases as the dendrite radius increases while it increases with increase in ER radius. Similar trend is observed in wave velocity (See subfigures 3.7b, 3.7d) where it increases with increasing ER radius and decreasing Dendrite radius.



(a) Amplitude change w.r.t RyR density and dendrite radius (b) Velocity change w.r.t RyR density and dendrite radius



(c) Amplitude change w.r.t RyR density and ER radius (d) Velocity change w.r.t RyR density and ER radius

Figure 3.7: Effects of RyR density on amplitude and velocity

Additionally, we see that there is a strong positive correlation of 0.97 between wave velocity and amplitude as seen in the figure 3.8.

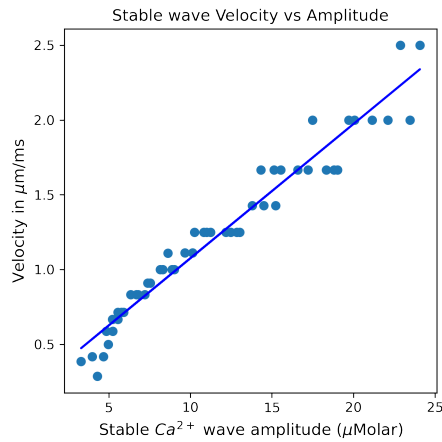


Figure 3.8: Strong correlation between wave amplitude and velocity

From these results, we expect the wave to be progressing faster in the thinner sections of the neuron and slower in thicker parts of the neuron (especially Soma).

## 3.7 Wave behaviour

### 3.7.1 Merging waves

In real neurons, with multiple synaptic activation, two waves originating at different ends may end up meeting at a point. In order to understand the nature of this meeting of waves, we simulated the cable neuron with activation at both left and right ends. The wave meets in the center and cancels each other effects. This is seen in left side figure of 3.9. The neuron cable initially shows low cytosolic Ca<sup>2+</sup> concentration indicated by dark blue color. As the activation occurs on both ends, the wave progression is seen by warmer colors indicating rise in Ca<sup>2+</sup> levels. As the two waves meet in center, the progression cancels out and the cable again settles to low levels of cytosolic Ca<sup>2+</sup>. The right side of figure 3.9 shows ER Ca<sup>2+</sup> concentration in the cable neuron.

Initially, the concentration is very high indicated by red color. As the wave starts on both ends, the concentration drops indicated by cooler colors as the wave progress. This is due to transport of ER  $\text{Ca}^{2+}$  to cytosol. As the left wave meets the right, there is very little to no ER  $\text{Ca}^{2+}$  left for progressing left wave. Same thing happens with wave approaching from the right. This exhaustion of  $\text{Ca}^{2+}$  in ER stalls the wave progression on both end. As seen in 3.4c, the replenishment of  $\text{Ca}^{2+}$  in ER is very slow further dampening the wave and cancelling it altogether.

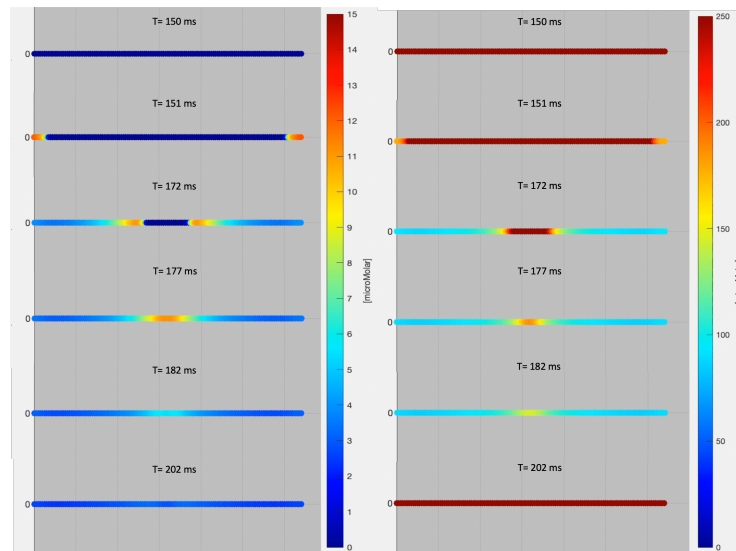
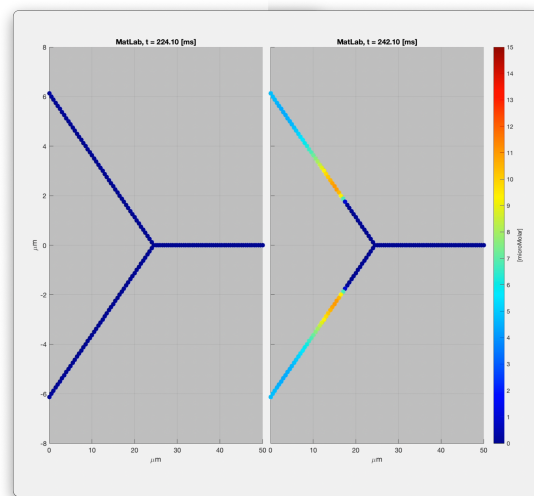


Figure 3.9: Calcium wave initiated on both end meeting at the center. *Left:* Cytosolic  $\text{Ca}^{2+}$  concentration evolution over time in cable neuron. *Right:* ER  $\text{Ca}^{2+}$  concentration evolution over time in cable neuron

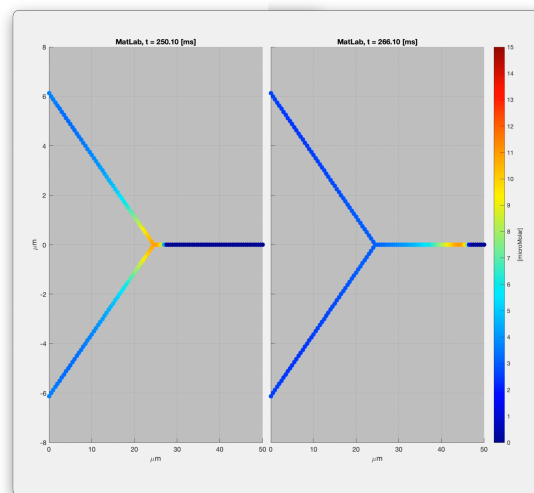
### 3.7.2 Y-shaped neuron geometry

In real neurons, there are branch points where waves could meet or one branch acts as influx and others as efflux. To test this, we created a Y-shaped geometry with two branches (each  $L = 32\mu\text{m}$ ) merge with to a common branch of  $L = 32\mu\text{m}$ . In first experiments, both the branch points were

activated to initiate  $\text{Ca}^{2+}$  waves in both branches. The wave progression for this experiment is seen in figure 3.10. In subfigure 3.10b left hand side, we see two waves meeting and progressing in the common branch. unlike in previous section where two meeting waves stalls each other, here the meeting waves have a path where the ER  $\text{Ca}^{2+}$  reserves are not exhausted (i.e. common branch). We also see that the amplitude of the wave in common branch is same as amplitude in individual branches. Merging of waves does not affect the wave amplitude or velocity in common branch.



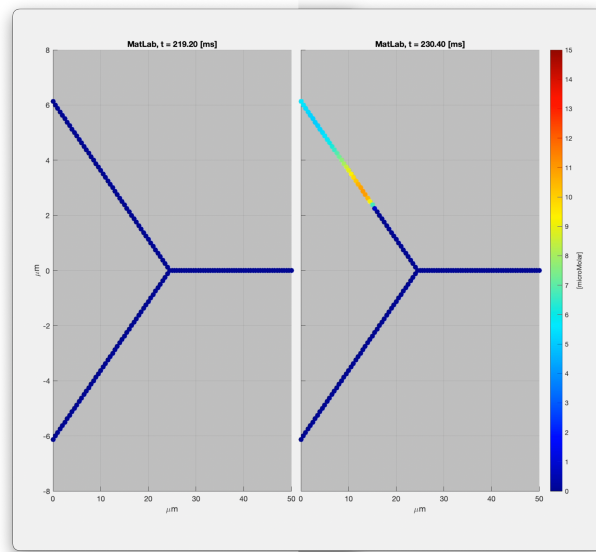
(a) *left*: Equilibrium state, *Right*: Activation or triggering of end point at two branches



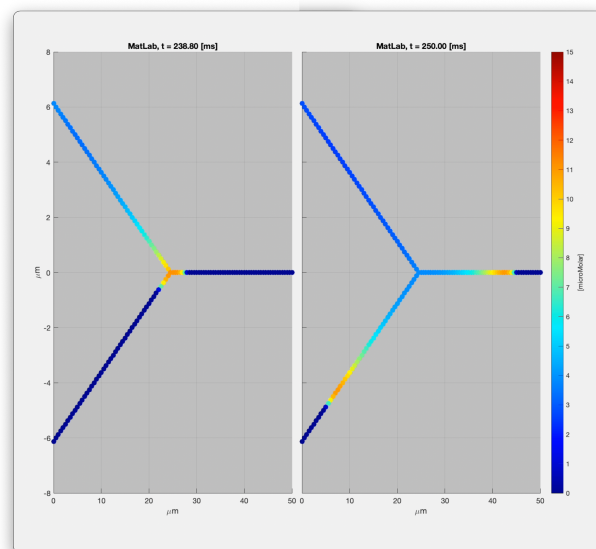
(b) *left*: Merging of two waves at the connection, *Right*: Progression of wave in common branch

Figure 3.10: Wave progression in Y-shaped geometry when two end points are triggered

We conducted another experiment in which only one branch is triggered allow wave progression from one branch to connection point. This can be seen in subfigure 3.11a right side. In subfigure 3.11b left side, we notice that the wave splits after arriving at the connector point. The splitting of wave in other branch and common branch causes wave progression with same amplitude and velocity as in the original wave.



(a) *left*: Equilibrium state, *Right*: Activation or triggering of end point of top branch



(b) *left*: Splitting of wave in bottom and common branch, *Right*: Progression of wave in bottom and common branch

Figure 3.11: Wave progression in Y-shaped geometry when one end point is triggered

These observations are important in understanding  $\text{Ca}^{2+}$  signalling in real geometry. We can expect that even if a wave is triggered at one spot in neuron, it will spread all around the neuron if given enough time.

### 3.8 Real neuron geometry

To summarise the three main observations in sections earlier, we learn that

1. Wave velocity and amplitude at a point will depend on dendrite ratio at that point in neuron,
2. two or more waves approaching towards each other will cancel each other out if there is no waveless path available to progress and
3. at branching points, the wave will split into all branches connected to the common node.

For the experiment 5 real neuron geometries were obtained from James Rosado (see Implementation chapter). To study wave progression and cumulative effect of various calcium waves at soma, for each geometry, we randomly selected 10, 5 and 1 points on the neuron. Once activated, the wave is allowed to progress until the wave covers the entire neuron. The cytosolic  $\text{Ca}^{2+}$  concentration profile over time for soma for each of the cells. This is presented in figure 3.12 where each subfigure correspond to a neuron cell. We first notice that the soma profile for all cells appears similar. The difference associated with amplitude reached can be attributed to difference in radius at soma point for all cells. Furthermore, in each cell, triggering 10, 5 or 1 point does not change the profile in any way. The only difference is time lag. However, this is understandable as the trigger points location can vary with some being closer to soma and other being away. This is particularly seen in subfigure 3.12c where one of the 10 or 5 points were closer to soma, but the single trigger point (green) was randomly picked at a distance away from soma. From this experiment, we see that a single trigger or multiple trigger elicit same response

at soma. This is not unexpected as we know that if a wave passes a point, it exhausts ER  $\text{Ca}^{2+}$  stores followed by very slow replenishment. This cancels out any other  $\text{Ca}^{2+}$  wave approaching that point.

For visualizing calcium wave progression in real neuron geometry we create video file with script provided by James Rosado. Figures 3.13 – 3.14 provides screenshots of the wave progression for neuron cell geometries *Cell 1*, *Cell 2*, *Cell 3*, *Cell 4* and *Cell 5*. For demonstration, videos for 5 trigger points were created. Going from left to right in each figure, we see that as the waves initiates, it passes through each point in neuron.

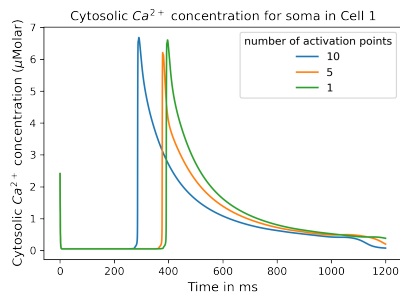
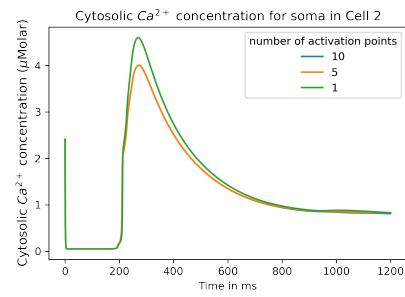
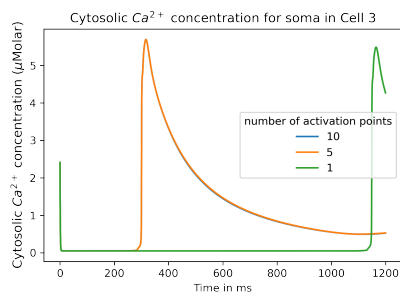
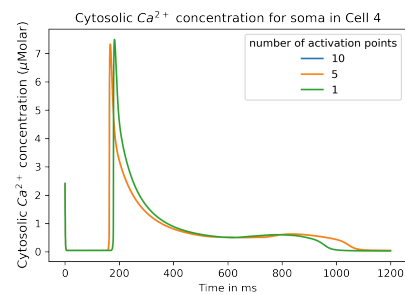
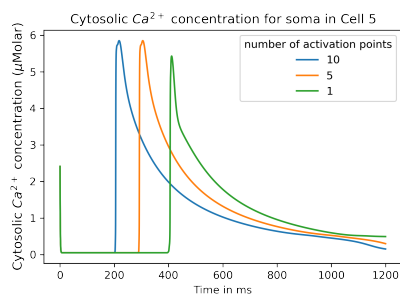
(a)  $\text{Ca}^{2+}$  profile in Cell 1(b)  $\text{Ca}^{2+}$  profile in Cell 2(c)  $\text{Ca}^{2+}$  profile in Cell 3(d)  $\text{Ca}^{2+}$  profile in Cell 4(e)  $\text{Ca}^{2+}$  profile in Cell 5

Figure 3.12: The cytosolic  $\text{Ca}^{2+}$  concentration profiles at soma for 5 real neuron cell geometries. Each cell was triggered with randomly selected 10, 5 and 1 points

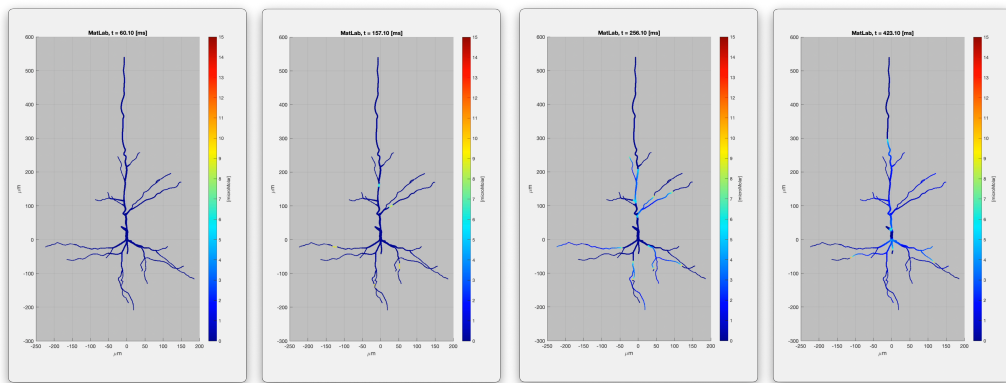


Figure 3.13: Wave progression with 5 trigger points in Cell 1

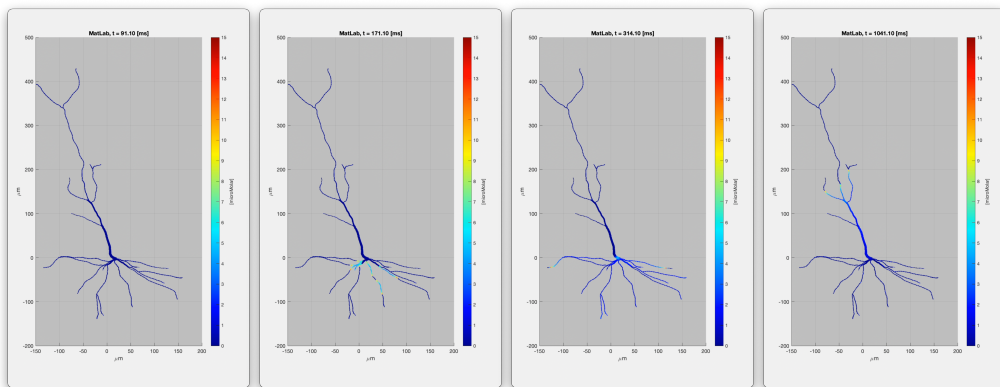


Figure 3.14: Wave progression with 5 trigger points in Cell 2

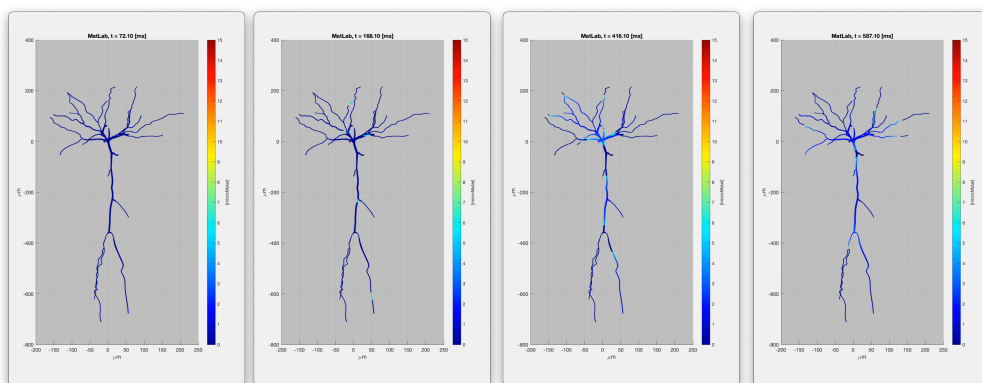


Figure 3.15: Wave progression with 5 trigger points in Cell 3

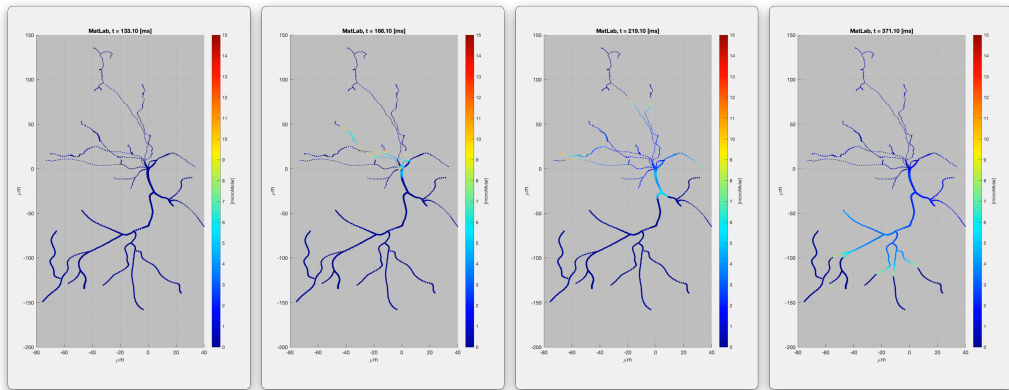


Figure 3.16: Wave progression with 5 trigger points in Cell 4

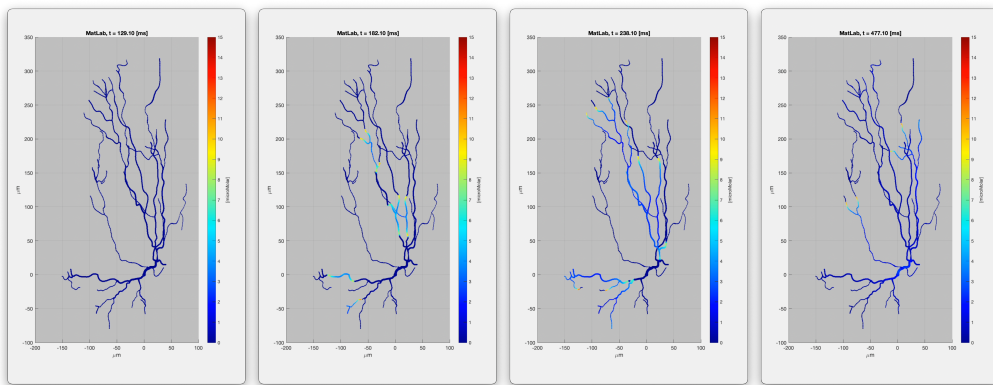


Figure 3.17: Wave progression with 5 trigger points in Cell 5

# CHAPTER 4

## CalciumSim simulator

### 4.1 Introduction

CalciumSim is a calcium simulator which models  $\text{Ca}^{2+}$  dynamics in three-dimension neuron geometries. CalciumSim is implemented in Matlab which implements the  $\text{Ca}^{2+}$  diffusion equations and pumps mechanisms explained in the introduction section. Figure 4.1 shows the flow of the simulator and various functions developed. The files “readSWC.m”, “getGraphStructure.m” and “makeMatlabMovCalcium.m” marked in red boxes are obtained from “<https://github.com/jarosado0911/Hodgkin-Huxley-MatLab-Repo>” authored by James Rosado. The program accepts neuron file and simulation run time in “CalciumSim.m”. This program pass file to “stencilMakerCalcium.m” to create a stencil matrix for the diffusion equations as described in 2.34. The “stencilMakerCalcium.m” utilizes “readSWC.m” and “getGraphStructure.m” files to read from “.swc” files. The “CalciumSim.m” also initializes cytosolic  $\text{Ca}^{2+}$ , ER  $\text{Ca}^{2+}$ , CalB and  $\text{IP}_3$  concentration at  $t = 0$  and sets step sizes for ODE solvers. “CalciumSim.m” also allows us to either select activation point or randomly creates activation points on neuron geometry. The stencil and initial values are passed on to “coupledEquations.m” file which carries out PDE integration.

“coupledEquations.m” first obtains fluxes generated by pumps and leak-

age mechanisms (“pumpEquations.m”, “IP3REquations.m” and “RyREquations.m”). The “pumpEquations.m” and “IP3REquations.m” takes cytosolic  $\text{Ca}^{2+}$ , ER  $\text{Ca}^{2+}$  and  $\text{IP}_3$  concentration to return flux values for SERCA, NCX, PMCA, two leakage and  $\text{IP}_3\text{R}$  channels. “RyREquations.m” uses backward Euler in “Euler.m” file to solve ODE and returns RyR channel flux. The “coupledEquations.m” then passes these values to “Euler.m” which utilizes forward Euler to calculate cytosolic  $\text{Ca}^{2+}$ , CalB, ER  $\text{Ca}^{2+}$  and  $\text{IP}_3$  concentrations at next time step. The derivative function for diffusion equations is obtained from “diffusionEquation.m” which also determines the activation flux values for  $\text{Ca}^{2+}$  and  $\text{IP}_3$  in cytosol. Once the simulation is completed, the four concentration values (namely cytosolic  $\text{Ca}^{2+}$ , ER  $\text{Ca}^{2+}$ , CalB and  $\text{IP}_3$  concentrations) for all time steps are saved in “ySol.mat” file for all points on neurons. There is also an option to store flux values for any pump mechanism for all time steps and points in neuron. This “ySol.mat” along with the respective “.swc” file can be passed to “makeMatlabMovCalcium.m” (from “James’s” code) to create a movie to visualize calcium movement in the neuron.

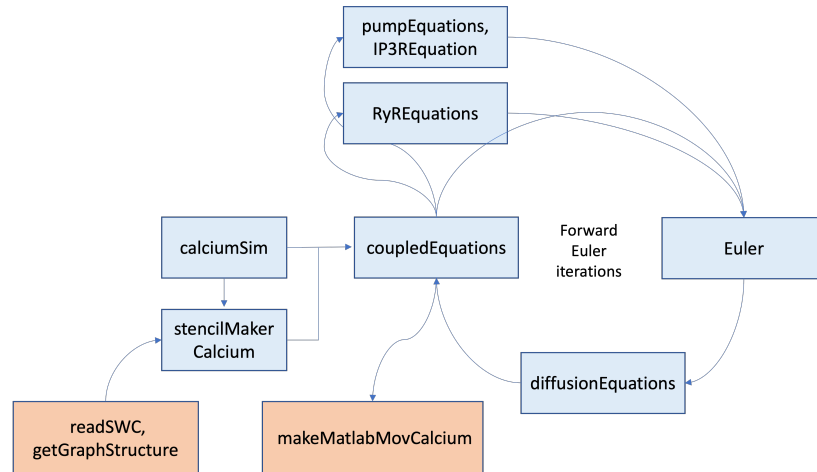


Figure 4.1: Flowchart of CalciumSim: The red boxes indicates files from another author

## 4.2 “.swc” file

The website “<http://neuromorpho.org/>” [1] maintains a database of 160598 neuronal cell geometries across various species and regions of nervous system. The geometry files are contributed by researchers from all around the world and are stored in special format called as “.swc” files. The file contains points matrix with seven columns. Each of columns are described in “<https://neuroinformatics.nl/swcPlus/>” -

1. *SampleID*: point identifier
2. *TypeID*: This identify the type of point it is. The values are described as follows -
  - -1: root
  - 0: undefined
  - 1: soma
  - 2: axon
  - 3: (basal) dendrite
  - 4: apical dendrite
  - 5+: custom
3. *x*: x-axis coordinates in  $\mu\text{m}$
4. *y*: y-axis coordinates in  $\mu\text{m}$
5. *z*: z-axis coordinates in  $\mu\text{m}$
6. *r*: Radius of dendrite at that point in  $\mu\text{m}$
7. *ParentID*: SampleID of the parent node

The files “readSWC.m” and “getGraphStructure.m” provided by James Rosado accept these files and creates adjacent matrix and provides various

statistics such as average edge length. “makeMatlabMovCalcium.m” also takes in “.swc” file to plot the neuron in three-dimensional geometry and then show the wave progression over time.

The neuron geometries, named below, used in this study were also provided by James Rosado. He obtained these geometries from “<http://neuromorpho.org/>”. The geometries were coarse than the acceptable step size for CalciumSim PDE evolution. Therefore, he created refinements by interpolations such that maximum distance between any two adjacent points was no more than  $1\mu m$  which is the acceptable spatial step size.

1. Cell 1: 228-16MG.CNG\_segLength=8\_1d\_ref\_1.swc
2. Cell 2: 0-2a.CNG\_segLength=8\_1d\_ref\_1.swc
3. Cell 3: 228-13MG.CNG\_segLength=8\_1d\_ref\_1.swc
4. Cell 4: M18-mPFC-4.CNG\_segLength=12\_1d\_ref\_2.swc
5. Cell 5: 194-4-17nj.CNG\_segLength=12\_1d\_ref\_2.swc

While “.swc” file provided radius of the dendrite, radius for ER is not provided. From the ER/dendrite radius ratio experiment, a ratio of 0.375 was selected to create a new vector of ER radius.

### 4.3 $v_{l,e}$ , $v_{l,p}$ calculator

The  $v_{l,e}$  and  $v_{l,p}$  are the velocities associated with the leakage flux  $j_{l,e}$  and  $j_{l,p}$  respectively (See equations 1.7 and 1.8). The velocities are calculated such that the net flow across Endoplasmic Reticulum membrane and Plasma membrane is zero at equilibrium. That is, when  $c_o = 1\text{ mM}$ ,  $c_c = 0.05\ \mu M$  and  $c_e = 250\ \mu M$

$$v_{l,e} = \frac{(j_S - j_R - j_I)}{(c_e - c_c)} \quad (4.1)$$

$$v_{l,p} = \frac{(j_N + j_P)}{(c_o - c_c)} \quad (4.2)$$

Calculating the values we find that  $v_{l,e} \approx 3.78e - 11$  and  $v_{l,p} \approx 4.49e - 12$ . However, it was noted that the exact value for  $v_{l,e}$  as calculated by Matlab is  $v_{l,e,exact}$ . In Matlab, due to limited precision, not all numbers are stored as exact values. For instance,  $v_{l,e} = 3.785e - 11$  is stored as  $v_{l,e,approx}$  in Matlab. Therefore, if  $v_{l,e} = 3.785e - 11$  is used instead of  $v_{l,e,exact}$ , a small leakage flux is created causing ER  $Ca^{2+}$  to constantly leak into cytosol. This leakage can be seen in figure 4.2 where  $v_{l,e,exact}$  and  $v_{l,e,approx}$  is used to compare. Although the error  $v_{l,e,exact} - v_{l,e,approx} = \epsilon = 2.1608671e - 15$  is negligible, it still leads to decrease in ER  $Ca^{2+}$  concentration which further leads to instability as the simulation progress. In order to circumvent this issue, a “vlevlpCalculator.m” file was created which returns exact values of  $v_{l,e}$  and  $v_{l,p}$  when provided with desired equilibrium conditions. These can be loaded in “pumpsEquations.m” directly while calculating leakage flux in order to avoid human error.

$$\begin{aligned}
 v_{l,e,exact} &= 3.78521608671366254486342512326204831 \\
 &\quad 62971680712871602736413478851318359375e - 11 \\
 v_{l,e,approx} &= 3.784999999999999724951795416202167312 \\
 &\quad 4305376489928676164709031581878662109375e - 11 \\
 \epsilon &= 2.1608671e - 15
 \end{aligned}$$

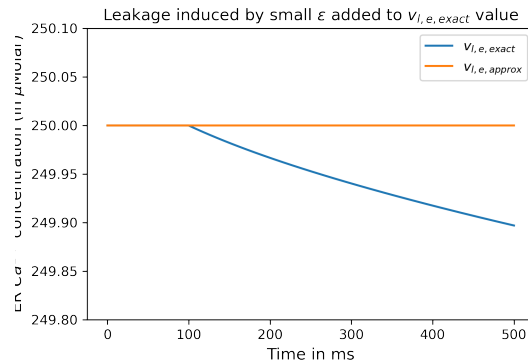


Figure 4.2: Constant ER  $\text{Ca}^{2+}$  concentration at  $250\mu\text{M}$  is seen when  $v_{l,e,exact}$  is used. Using  $v_{l,e,approx}$  leads to constant decrease in ER  $\text{Ca}^{2+}$  concentration

## 4.4 time complexity

While the test geometries consisted of 100 – 200 points, the real neuron geometries contains more than 1000 points. This adds to run time for the simulation. In order to understand how run time is affected by number of points, neuron geometries with 2, 4, 8, 16, 32, 64, 128, 256, 512, 1024, 2048, 4096 points. A series 1000 milliseconds (simulation time) simulations were performed with these geometries and run time was noted. The figure 4.3 shows that as the number of points increases, run time also increases linearly. Specifically, the slope obtained was 0.25, meaning the run time in seconds was  $0.25 \times$  number of points.

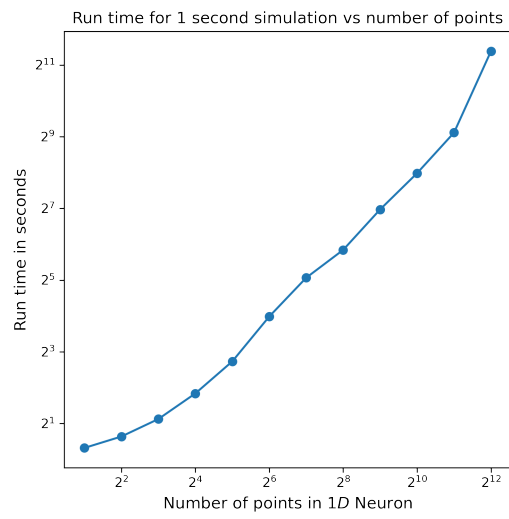


Figure 4.3: Time taken for one second of simulation on 1D neuron geometry made up of 2, 4, 8, 16, 32, 64, 128, 256, 512, 1024, 2048, 4096 points

# CHAPTER 5

## Conclusion

“CalciumSim” is a user friendly  $\text{Ca}^{2+}$  dynamics simulator created to study  $\text{Ca}^{2+}$  signalling in real neuron geometry. It is a Matlab implementation which accepts “.swc” files and models calcium dynamics for that neuron geometry. Having implemented the calcium dynamics, comparison studies were done with existing literature to establish reliability of the implementation. Once convinced, we used this implementation to model on real neuron geometry and studied behavior of calcium wave. We derived important insights with respect to wave behaviour which are used to provides suggestions and future study directions here.

We identified the role of  $\text{IP}_3$  molecule in sustenance of the wave. The fact that quick decay of  $\text{IP}_3$  molecule is extremely important for neuron to reach equilibrium again can form a potential therapeutic target. Constant activation of neurons without real triggers quickly leads to neuro-degeneration. In order to avoid this, targeting  $\text{IP}_3$  molecule to decay it faster may save the neuron from damage and eventual apoptosis.

In tau pathology associated (Alzheimer’s’ disease) neurodegeneration, the synapses are blocked reducing the calcium signalling needed for transcribed genes for protection and memory. With “CalciumSim” one can model this behavior by first simulating conditions leading to weakening signal to soma and then modulating other parameters such as RyR density to obtain original

signal profile. This can help identify various therapeutic targets such as RyR channels.

Another conclusion we draw is that stable  $\text{Ca}^{2+}$  wave is highly dependent on ER  $\text{Ca}^{2+}$  stores. A quick replenishment of ER  $\text{Ca}^{2+}$  is vital for any new wave progression. Recent studies have shown certain pathways which connects ER to extracellular  $\text{Ca}^{2+}$  reserves bypassing cytosol [29]. This mechanism maybe involved in quick replenishment of ER and needs to be studied. Future work would involve adding such component to “CalciumSim”. “CalciumSim” allows easy integration of new components to current code base thereby allow one to study wave propagation under various conditions.

Further work needs to be done to include multiple neuron structures to study network of neurons. This would lead to a realistic model for study signalling in neurons. While calcium signalling is biochemical signalling pathway, the primary mode of signalling between neurons is electrical. Therefore, future work would also focus on coupling Hodgkin-Huxley model for electric signal to calcium signalling.

Although addition of more components makes model more realistic, it however adds to computation cost. As the PDE equations for calcium signalling is a complex problem with multiple non-linear functions, developing a faster ODE solver is still an active area of research. With many components involved in the diffusion equations, an implicit-explicit scheme could be conceived to make computation faster.

Overall, “CalciumSim” provides fast, reliable and accurate modelling of calcium signalling which can be easily modified to suit a particular study condition and derived biologically important insights.

## REFERENCES

- [1] Giorgio A Ascoli. Mobilizing the base of neuroscience data: the case of neuronal morphologies. *Nature Reviews Neuroscience*, 7(4):318–324, 2006.
- [2] Michael J Berridge. Calcium microdomains: organization and function. *Cell calcium*, 40(5-6):405–412, 2006.
- [3] Ilya Bezprozvanny and Barbara E Ehrlich. Inositol (1, 4, 5)-trisphosphate (insp3)-gated ca channels from cerebellum: conduction properties for divalent cations and regulation by intraluminal calcium. *The Journal of General Physiology*, 104(5):821–856, 1994.
- [4] Ilya Bezprozvanny and Michael R Hayden. Deranged neuronal calcium signaling and huntington disease. *Biochemical and biophysical research communications*, 322(4):1310–1317, 2004.
- [5] Przemyslaw Bogacki and Lawrence F Shampine. An efficient runge-kutta (4, 5) pair. *Computers & Mathematics with Applications*, 32(6):15–28, 1996.
- [6] Markus Breit, Marcus Kessler, Martin Stepniewski, Andreas Vlachos, and Gillian Queisser. Spine-to-dendrite calcium modeling discloses relevance for precise positioning of ryanodine receptor-containing spine endoplasmic reticulum. *Scientific reports*, 8(1):1–17, 2018.

- [7] Markus Breit and Gillian Queisser. What is required for neuronal calcium waves? a numerical parameter study. *The Journal of Mathematical Neuroscience*, 8(1):1–22, 2018.
- [8] Dibyadeep Datta, Shannon N Leslie, Min Wang, Yury M Morozov, Shengtao Yang, SueAnn Mentone, Caroline Zeiss, Alvaro Duque, Pasko Rakic, Tamas L Horvath, et al. Age-related calcium dysregulation linked with tau pathology and impaired cognition in non-human primates. *Alzheimer's & Dementia*, 2021.
- [9] Gary W De Young and Joel Keizer. A single-pool inositol 1, 4, 5-trisphosphate-receptor-based model for agonist-stimulated oscillations in  $ca^{2+}$  concentration. *Proceedings of the National Academy of Sciences*, 89(20):9895–9899, 1992.
- [10] Paul Dierckx. An algorithm for smoothing, differentiation and integration of experimental data using spline functions. *Journal of Computational and Applied Mathematics*, 1(3):165–184, 1975.
- [11] J Kevin Foskett, Carl White, King-Ho Cheung, and Don-On Daniel Mak. Inositol trisphosphate receptor  $ca^{2+}$  release channels. *Physiological reviews*, 87(2):593–658, 2007.
- [12] Agnes Görlach, Peter Klappa, and Dr Thomas Kietzmann. The endoplasmic reticulum: folding, calcium homeostasis, signaling, and redox control. *Antioxidants & redox signaling*, 8(9-10):1391–1418, 2006.
- [13] Michael Graupner. *A theory of plasma membrane calcium pump function and its consequences for presynaptic calcium dynamics*. PhD thesis, Diploma thesis. Technische Universität Dresden, 2003.
- [14] Etsuro Ito, Kotaro Oka, Rene Etcheberrigaray, Thomas J Nelson, Donna L McPhie, Beth Tofel-Grehl, Gary E Gibson, and Daniel L Alkon. Internal  $ca^{2+}$  mobilization is altered in fibroblasts from patients with

- alzheimer disease. *Proceedings of the National Academy of Sciences*, 91(2):534–538, 1994.
- [15] Joel Keizer and Leslie Levine. Ryanodine receptor adaptation and  $ca^{2+}$  (-) induced  $ca^{2+}$  release-dependent  $ca^{2+}$  oscillations. *Biophysical journal*, 71(6):3477–3487, 1996.
- [16] Toshinori Kimura. On dormant-prince method. *Jpn. Malaysia Tech. Instit*, 40:1–9, 2009.
- [17] Klara Limbäck-Stokin, Edward Korzus, Rie Nagaoka-Yasuda, and Mark Mayford. Nuclear calcium/calmodulin regulates memory consolidation. *Journal of Neuroscience*, 24(48):10858–10867, 2004.
- [18] Philippe Marambaud, Ute Dreses-Werringloer, and Valérie Vingtdeux. Calcium signaling in neurodegeneration. *Molecular neurodegeneration*, 4(1):1–15, 2009.
- [19] Volker Nimmrich, Christiane Grimm, Andreas Draguhn, Stefan Barghorn, Alexander Lehmann, Hans Schoemaker, Heinz Hillen, Gerhard Gross, Ulrich Ebert, and Claus Bruehl. Amyloid  $\beta$  oligomers ( $a\beta_{1-42}$  globulomer) suppress spontaneous synaptic activity by inhibition of p/q-type calcium currents. *Journal of Neuroscience*, 28(4):788–797, 2008.
- [20] Yohei Okubo, Sho Kakizawa, Kenzo Hirose, and Masamitsu Iino. Visualization of  $ip_3$  dynamics reveals a novel ampa receptor-triggered  $ip_3$  production pathway mediated by voltage-dependent  $ca^{2+}$  influx in purkinje cells. *Neuron*, 32(1):113–122, 2001.
- [21] Sofia Papadia, Patrick Stevenson, Neil R Hardingham, Hilmar Bading, and Giles E Hardingham. Nuclear  $ca^{2+}$  and the camp response element-binding protein family mediate a late phase of activity-dependent neuroprotection. *Journal of Neuroscience*, 25(17):4279–4287, 2005.

- [22] Morgan Sheng, Grant McFadden, and Michael E Greenberg. Membrane depolarization and calcium induce c-fos transcription via phosphorylation of transcription factor creb. *Neuron*, 4(4):571–582, 1990.
- [23] Perry B Shieh, Shu-Ching Hu, Kathryn Bobb, Tonnis Timmusk, and Anirvan Ghosh. Identification of a signaling pathway involved in calcium regulation of bdnf expression. *Neuron*, 20(4):727–740, 1998.
- [24] J Sneyd, K Tsaneva-Atanasova, JIE Bruce, SV Straub, DR Giovannucci, and DI Yule. A model of calcium waves in pancreatic and parotid acinar cells. *Biophysical journal*, 85(3):1392–1405, 2003.
- [25] Marc Nico Spijker. Stiffness in numerical initial-value problems. *Journal of Computational and Applied Mathematics*, 72(2):393–406, 1996.
- [26] Peiqing Sun, Herve Enslen, Peggy S Myung, and Richard A Maurer. Differential activation of creb by ca<sup>2+</sup>/calmodulin-dependent protein kinases type ii and type iv involves phosphorylation of a site that negatively regulates activity. *Genes & development*, 8(21):2527–2539, 1994.
- [27] John L Sutko and Judith A Airey. Ryanodine receptor ca<sup>2+</sup> release channels: does diversity in form equal diversity in function? *Physiological Reviews*, 76(4):1027–1071, 1996.
- [28] XU Tao, Steven Finkbeiner, Donald B Arnold, Adam J Shaywitz, and Michael E Greenberg. Ca<sup>2+</sup> influx regulates bdnf transcription by a creb family transcription factor-dependent mechanism. *Neuron*, 20(4):709–726, 1998.
- [29] Nicholas C Vierra, Samantha C O’Dwyer, Collin Matsumoto, L Fernando Santana, and James S Trimmer. Regulation of neuronal excitation–transcription coupling by kv2. 1-induced clustering of somatic l-type ca<sup>2+</sup> channels at er-pm junctions. *Proceedings of the National Academy of Sciences*, 118(46), 2021.

- [30] Jörg Wensch, Karl Strehmel, and Rüdiger Weiner. A class of linearly-implicit runge-kutta methods for multibody systems. *Applied numerical mathematics*, 22(1-3):381–398, 1996.
- [31] Sheng-Jia Zhang, Ming Zou, Li Lu, David Lau, Désirée AW Ditzel, Celine Delucinge-Vivier, Yoshinori Aso, Patrick Descombes, and Hilmar Bading. Nuclear calcium signaling controls expression of a large gene pool: identification of a gene program for acquired neuroprotection induced by synaptic activity. *PLoS genetics*, 5(8):e1000604, 2009.